

Article

Assessing the Impact of Human Activities and Climate Change Effects on Groundwater Quantity and Quality: A Case Study of the Western Varamin Plain, Iran

Roza Asadi ^{1,*}, Mehraneh Zamaniannejatzadeh ¹ and Mehdi Eilbeigy ²¹ Department of Civil Engineering, K.N. Toosi University of Technology, Tehran 14176-14411, Iran² Faculty of Earth Science, Shahid Chamran University of Ahvaz, Ahvaz 61357-43311, Iran

* Correspondence: asadi@kntu.ac.ir

Abstract: In this paper, the effects of climate change and human activities on the groundwater level and the concentration of pollutants, such as total dissolved solids (TDS), chloride, and sodium, were investigated in the western part of the Varamin Plain. The groundwater flow and pollutant transport were simulated with the two models of MODFLOW and MT3D, respectively. To investigate the impacts of climate change, the two parameters of temperature and precipitation were downscaled under the three scenarios of RCP 2.6, RCP 4.5, and RCP 8.5. Four scenarios, including the current condition (Scenario 0), a 25% increase in the extraction from pumping wells (Scenario 1), the climate change effects (Scenario 2), and an increase in the incoming effluent (TDS) to the Shoor River due to industrial activities (Scenario 3), were investigated for a future period of 30 years (2025–2055). The results show that the highest groundwater decline and chloride and sodium concentrations occur under Scenario 1, while Scenario 3 leads to the maximum TDS concentration (milligrams per liter). In Scenario 1, the average and maximum groundwater decline at the end of the simulation period will be 2.5 m and 7.3 m, and the chloride and sodium concentrations will increase by 7 and 5 milligrams per liter, respectively.

Keywords: groundwater modeling; contaminant transport; climate change; total dissolved solids; chloride ion; sodium ion; Varamin Plain



Citation: Asadi, R.; Zamaniannejatzadeh, M.; Eilbeigy, M. Assessing the Impact of Human Activities and Climate Change Effects on Groundwater Quantity and Quality: A Case Study of the Western Varamin Plain, Iran. *Water* **2023**, *15*, 3196. <https://doi.org/10.3390/w15183196>

Academic Editor: Cesar Andrade

Received: 18 July 2023

Revised: 29 August 2023

Accepted: 2 September 2023

Published: 7 September 2023



Copyright: © 2023 by the authors. Licensee MDPI, Basel, Switzerland. This article is an open access article distributed under the terms and conditions of the Creative Commons Attribution (CC BY) license (<https://creativecommons.org/licenses/by/4.0/>).

1. Introduction

Groundwater refers to subsurface water that can be collected through wells, tunnels, and drainage galleries or can percolate to the surface naturally through seepage or springs. Groundwater is vital in various domains such as drinking, agriculture, industry, environment, and ecosystems. Groundwater reservoirs represent the largest source of accessible liquid freshwater on the planet [1] and supply approximately 36% of worldwide drinking water [2]. In arid and semi-arid regions, such as Iran, where the surface water is contaminated or scarce, the dependence upon groundwater is quite remarkable. Evidence shows that in the near future, factors including population growth and climate change, will result in the intensification of groundwater consumption [3].

Recent studies indicate that the quality and quantity of groundwater could be impacted by global climate change through the two parameters of temperature and precipitation [4–9]. Indeed, climate variation alters the distribution of temperature and precipitation around the world. The Intergovernmental Panel on Climate Change (IPCC) predicts a temperature increase of 2 to 4 degrees over the 21st century [10]. However, the change in the regime and quantity of precipitation is uncertain, but, generally, a decrease in dry zones and an increase in wet areas are forecasted [10].

Two direct consequences of temperature increases are increases in evapotranspiration and crop water need (CWN) [11–13]. Subsequently, these parameters, together with

precipitation, affect irrigation water need (IWN) [11–13] and, ultimately, change groundwater discharge because of the aquifer pumpage. Another key element that links climate variables to the groundwater system is recharge [5,7,14,15]. Indeed, precipitation and evapotranspiration directly influence the recharge value [14–18]. Allen et al. analyzed the sensitivity of the Grand Forks aquifer, located in British Columbia, Canada, according to the change in the recharge and river stage, as well as different climate projection scenarios. The results showed that the hydraulic head variations were insignificant and ranged between -0.025 m and 0.5 m for the lowest and highest recharge conditions, respectively [15]. In [17], the effect of climate change on groundwater recharge was investigated for eight aquifers in the western United States. The simulations indicated that in the southern parts, the recharge would decrease, while in the northern aquifers, a slight increase to low decline would be expected.

According to the issues mentioned above, accurate estimations for future projections of temperature and precipitation are essential. One of the most reliable tools to estimate future climate variables is the use of general circulation models (GCMs). These physically based computer models simulate climate response to IPCC scenarios [7]. In this study, scenarios from the fifth assessment report (AR5), including representative concentration pathways (RCPs), were considered to evaluate the impact of climate change on groundwater resources [19]. In the AR5, the four RCPs of 2.6, 4.5, 6, and 8.5 are presented according to the low, intermediate, and high greenhouse gas emission scenarios, respectively [19].

Since the Coupled Model Intercomparison Project Phase 5 (CMIP5) was conducted to support the AR5 by employing the RCP emission scenarios, and because of the higher spatial resolution and improved model physics, it was selected in this work [8]. Among the CMIP5 GCMs, the Canadian Earth System Model of the Canadian Centre for Climate Modeling and Analysis (CanESM2) [20,21] was used in the current study to select the appropriate predictors. The so-called GCM model approximately matches the resolution of the NCEP/NCAR reanalysis data [21,22] and has been successfully applied in many cases [23–25]. Furthermore, to resolve the GCM outputs on a regional scale, statistical downscaling techniques are commonly applied as an effective and computationally inexpensive tool [26]. Indeed, to provide station-scale climate information, an empirical relationship is established between local predictands and large-scale GCM predictors [26]. In this study, SDSM 4.2 (statistical downscaling model) software was employed in which multiple linear regression was used for temperature and precipitation projection [27]. This software has been widely used, and it is a reliable tool for downscaling climate data [28–33].

In addition to the climate change effect, human activities play a significant role in the fluctuations in groundwater levels and the quality of this resource. In order to implement both the human-made and climate change scenarios, the flow model of MODFLOW [34–36] and solute-transport model of MT3DMS [37] were used in this study to evaluate the groundwater level and pollutants concentrations, respectively. For this purpose, the groundwater modeling system (GMS) simulation software was employed to integrate these two models and facilitate the pre- and postprocessing via three-dimensional visualization [38].

Despite the growing research in recent years investigating the impact of climate change on groundwater resources, there are a limited number of studies focusing both on groundwater quantity and quality [39]. This is because of the fact that, contrary to surface water, which can easily be measured and monitored, a groundwater system's response to both human-made and climate change scenarios is very complicated [39]. Therefore, in the present study, a conceptual modeling approach was developed to integrate the groundwater drawdown, pollution, climate change scenarios, and anthropogenic factors to assess future groundwater conditions. Moreover, in most studies, the impact of climate change on groundwater resources is considered through the recharge process or direct interaction with surface water [5,7]. In the methodology proposed in this study, in addition to the effect of recharge, the variation in irrigation water need and the consequent discharge under future climate scenarios is estimated.

The study area considered in this work is the Varamin Plain, located in Iran, southeast of Tehran Province. The agricultural lands in this plain cover more than 60,000 ha and play a crucial role in providing agricultural products [40]. This leads to excessive groundwater extraction and groundwater level decline [41]. On the other hand, since the climate of this zone is dry with low precipitation and high temperature, climate change could increase the drought and affect groundwater resources in future decades [40,42]. Based on the studies performed in this plain, the total dissolved solids (TDS) exceeds 1000 milligrams per liter (mg/L) in the western part of the area [40], which is categorized as brackish groundwater [43]. As a result, overpumping and climate alteration could significantly deteriorate the salinity conditions of the groundwater supply in this region. Hence, in the current research, the concentration of TDS, chloride, and sodium ions were considered to examine the salinity characteristics of the study area.

In recent studies conducted in the Varamin Plain, the effect of climate change on runoff using a soil and water assessment tool (SWAT) was investigated. The results show an increase in the runoff in the fall and spring and a decrease in the winter and summer for all scenarios [42]. Furthermore, Azizi et al. (2021) evaluated the effect of climate change on the groundwater level in the Varamin Plain under RCP scenarios. In this study, the general circulation model (GCM) of the EC-EARTH and the downscaling model of the LARS-WG were applied. The downscaled model showed an increase in temperature up to 1.5 degrees between the future periods of 2020 and 2050 [44]. Azizi (2023) developed a simulation-optimization model in the Varamin aquifer to select a sustainable harvesting plan for this plain. In this paper, the Borda aggregation method was applied to select the best solution for aquifer management [45]. For the qualitative studies performed in the Varamin Plain, Karami et al. (2018) used the kriging method to interpolate groundwater quality data, including total dissolved solids (TDS), sodium adsorption ratio (SAR), electrical conductivity (EC), sodium, total hardness, chloride, and sulfate, in the Varamin Plain [46]. The study attempted to determine zones with low and high groundwater quality due to the high value of TDS and threat of salinity in recent years [46]. In another work, Valivand and Katibeh (2019) simulated nitrate pollution in the Varamin aquifer by coupling the two models of MODFLOW and MT3DMS. In this study, the concentration of nitrate was predicted until 2041 under existing conditions [41]. To date, according to the authors' knowledge, no study has included the following issues: (1) modeling the three pollutants of TDS, chloride, and sodium simultaneously in the study area; (2) investigating the impact of climate change on the quality characteristics of the Varamin Plain; (3) considering the climate change effect on crop water need and the resultant pumpage in this zone; and (4) the human-based scenarios applied in this study.

The main objectives of this work were as follows: (1) estimate the future projection of temperature and precipitation with the coupled GCM and statistical downscaling method under the RCP scenarios; (2) compute the future groundwater decline and spatiotemporal distribution of pollutants under the current condition; and (3) investigate the effect of climate change and possible human-based scenarios via the proposed methodology.

2. Materials and Methods

2.1. Study Area

The Varamin Plain is located in the southeast of Tehran Province, with the minimum and maximum heights of 810 m and 2310 m, respectively (Figure 1). The main sources of water in the Varamin Plain include the Jajrood River, Shoor River, sewers of the south of Tehran, and groundwater, which are utilized for both drinking and irrigation demands. The whole plain is characterized by an arid climate, with minimum and maximum temperatures of 8.5 °C and 24.2 °C, respectively. The annual rainfall ranges between 193 mm in the northern uplands and 143 mm in the southern lowlands. In addition, the average annual precipitation is approximately 160 mm. The Varamin Plain plays a leading role in agriculture as the supplier of agricultural products for Tehran and other parts of the country. The dominant cultivations are barley, wheat, corn, and alfalfa [47].

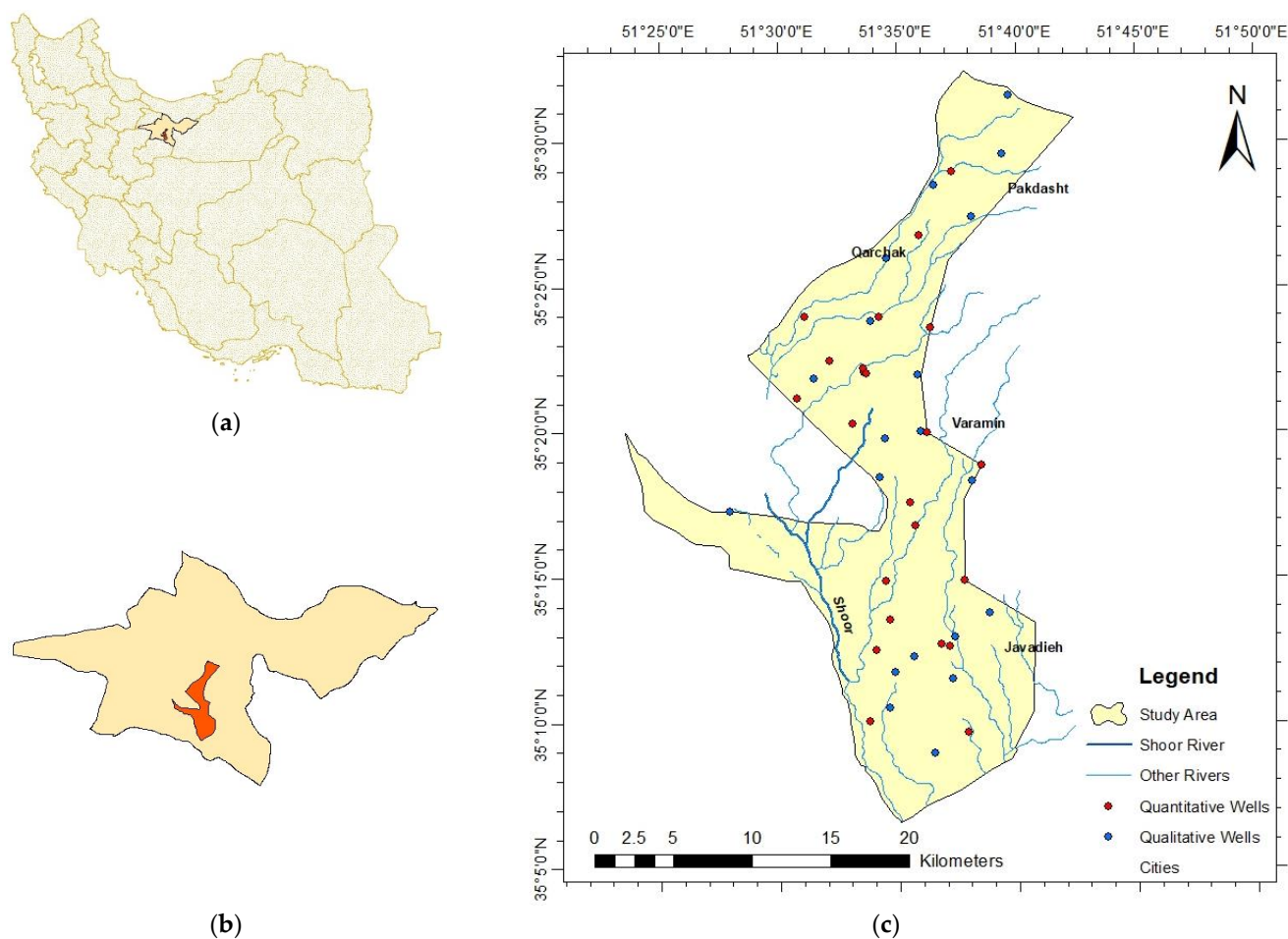


Figure 1. (a) Iran; (b) Tehran Province; (c) location map of the study area.

The wide area of the plain is managed by the Varamin Irrigation and Agriculture Network, and the water is supplied from the wastewater of the Tehran sewage treatment plant. Furthermore, wastewater from the treatment plant in the southeast of Tehran is transferred to the Varamin Plain and enters the irrigation network. This network recharges the aquifer; therefore, recursive flows import pollutants to it [41]. Additionally, the pollutants that enter the Shoor River and industrial wastewater increase the values of TDS in the western and southern parts of the plain, as shown in Figure 2. In this study, the western part of the Varamin was considered the study area because the concentration of TDS exceeds the permissible limit (by more than 1000 mg/L, according to a World Health Organization report [43]) in this zone. Also, samples from the monitoring wells in a field site show that among the measured solute components, the concentration of chloride (Cl^-) and sodium (Na^+) are the highest. According to irrigation activities in this area, the salinity could impact the groundwater quality and be a potential for deterioration of groundwater in the future. Therefore, the concentration of the three parameters of TDS, chloride, and sodium were investigated in this research.

The area of the model domain was approximately 430 km² between the east longitudes of 51°20' and 51°45' and north latitudes of 35°6' and 35°38'. Hydrogeology studies show that the aquifer under consideration is composed of soils with a wide grain size distribution (from coarse gravel to a mixture of sand and clay), which demonstrates the large spatial variation in hydraulic properties. Figure 1 shows the study area's location and the model domain's layout in Iran and Tehran Province [47].

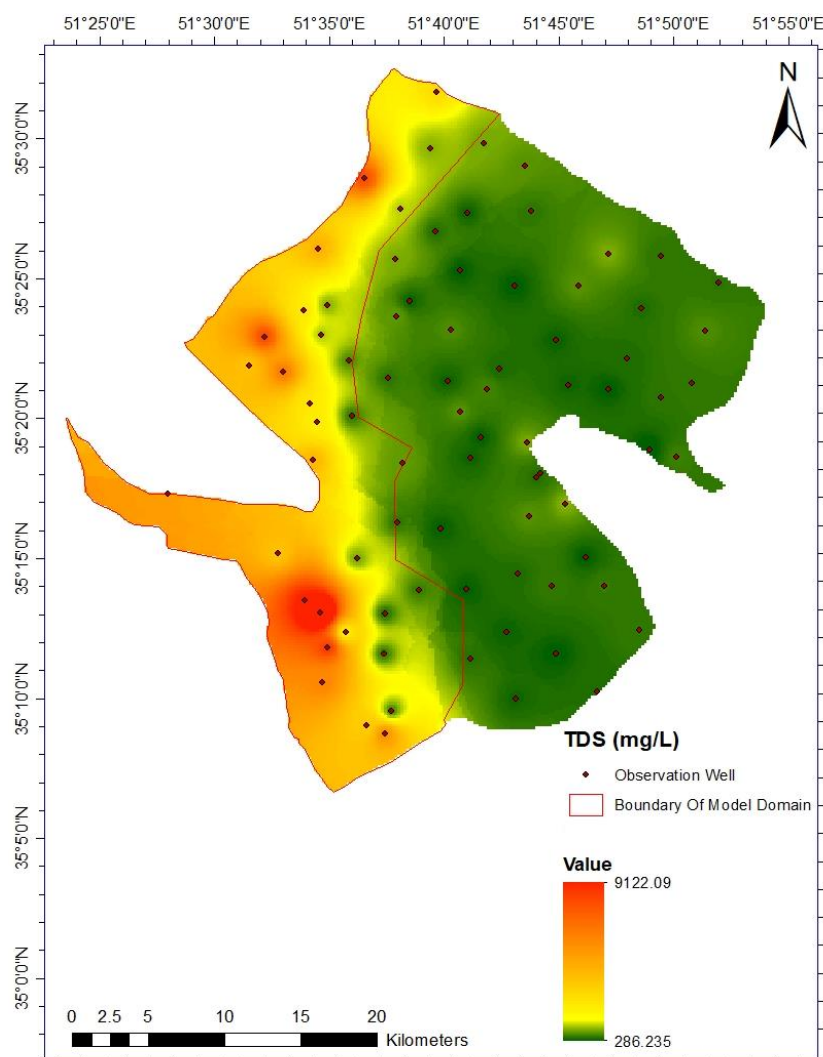


Figure 2. The boundary of the model domain.

2.2. General Framework of Modeling

The general framework of the proposed model is presented in Figure 3. As shown in the figure, the climate change scenarios are projected according to the two parameters of temperature and precipitation. In the next step, the variation in the reference evapotranspiration and crop water needs are calculated. Then, the irrigation water need is computed via the effective precipitation and crop water need. The alteration in the irrigation water need in response to the climate change results in an increase in pumpage. Meanwhile, the change in recharge due to the forecasted precipitation is applied to the groundwater flow model. Finally, human-based and climate change scenarios are employed in the contamination groundwater model to determine the concentrations of pollutants.

2.3. Models Used in Quantitative and Qualitative Simulation

In this research, the MODFLOW and MT3DSMS models in GMS software were used to solve the governing equations of the groundwater flow and contaminant transport, respectively, using the finite difference numerical method. The two models interface directly with the same mesh layout. Indeed, the qualitative data, including the head distribution and velocity field, were imported into the MT3DMS model to compute the contaminant concentration and identify the sources and causes of pollution in the aquifer [37].

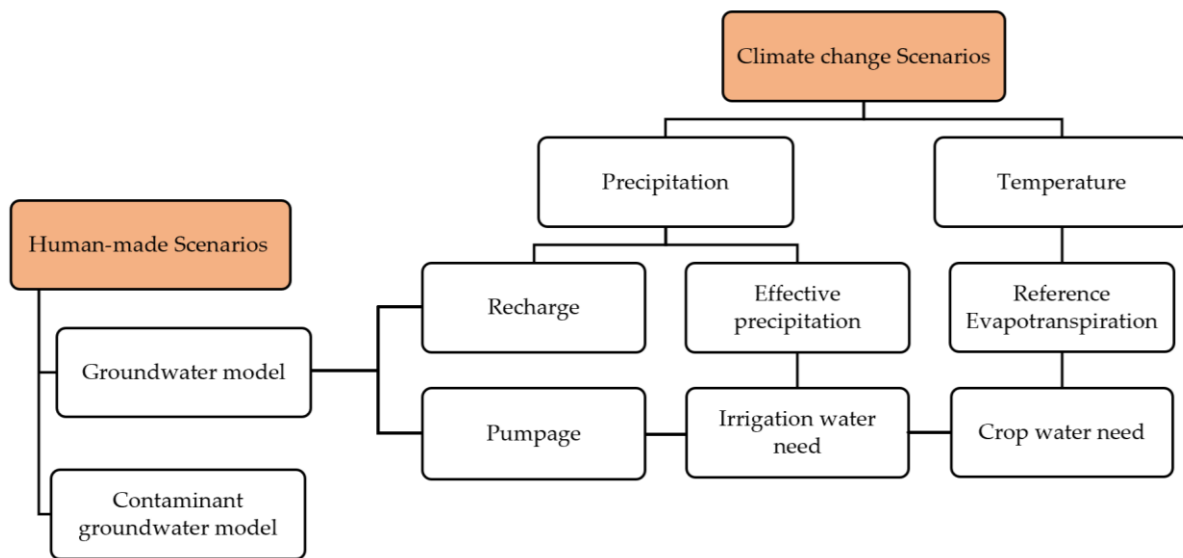


Figure 3. The general framework of modeling.

In this framework, a general governing equation for the groundwater flow in an anisotropic, heterogeneous aquifer can be written as follows:

$$\frac{\partial}{\partial x_i} \left(K_{ij} \frac{\partial h}{\partial x_j} \right) + w = S_S \frac{\partial h}{\partial t} \tag{1}$$

where K_{ij} is the second-order tensor of hydraulic conductivity, h denotes the hydraulic head, x_i are the cartesian coordinates, w is the volumetric flux per unit volume representing the sources and sinks terms, S_S is the specific storage of the investigated aquifer, and t is the time. By solving the above equation in MODFLOW, the hydraulic head values and velocity values are calculated.

For the MT3DMS model, the partial differential equation describing the three-dimensional single solute transport can be expressed as follows [37,48]:

$$\frac{\partial(\theta C)}{\partial t} = \frac{\partial}{\partial x_i} \left(\theta D_{ij} \frac{\partial C}{\partial x_j} \right) - \frac{\partial}{\partial x_i} (\theta v_i C) + q_s C_s + \sum R_n \tag{2}$$

where C is the dissolved pollutant concentration, θ is the porosity of the medium, D_{ij} is the hydrodynamic dispersion coefficient tensor, v_i is the seepage or linear pore water velocity based on Darcy’s law, q_s is the volumetric flow rate per unit volume of aquifer representing fluid sources and sinks, C_s is the concentration of sources or sink flux, and $\sum R_n$ represents the chemical reaction term [48].

In this research, the mechanisms of advection and hydrodynamic dispersion are considered, which are given in the first and second terms of Equation (2), respectively, and the chemical reactions are neglected.

2.4. Primary Information of Groundwater Flow Modeling

In the study area, the aquifer is unconfined and considered a one-layer model. The boundary condition of the simulated domain was defined based on the groundwater isoline map, geology, and location of the observation wells. Preparing and solving the mathematical model of an aquifer using the finite difference method requires the division of the layer into grids, components, or smaller rectangular or square cells. According to the previous models applied in this study area [41,45], the model grid of the Varamin aquifer was divided into regular and equal-sized cells of 250 m × 250 m (Figure 4). Figure 4 also shows the permeable and impermeable boundaries as well. Moreover, according to the

field data, the porosity was considered to be 0.3, and the groundwater level and depth were assumed from [47].

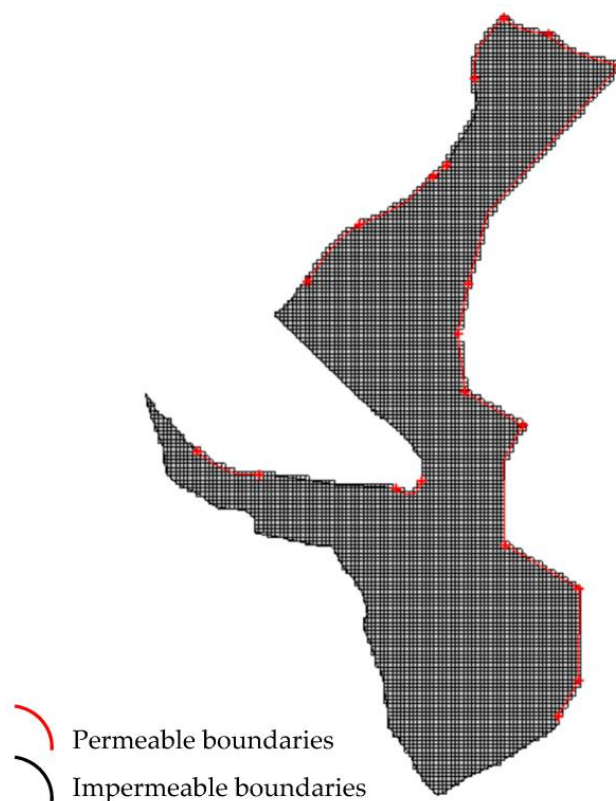


Figure 4. Area's cells with the boundary condition.

As shown in Figure 4, two boundary types, including permeable and impermeable, were applied in the quantitative and qualitative models. The impermeable boundaries were assigned based on the groundwater level isolines and geological formations. As depicted in Figure 5, where the groundwater level isolines are perpendicular to the boundary, it is considered an impermeable surface. Furthermore, in the zones with a lack of observation wells (i.e., the western part of the study area), the geological data were investigated, and in the interface of the Varamin Plain and mountains, a no-flow boundary condition was assumed. In the permeable boundaries, the constant and time-variant heads were considered in the steady-state and transient quantitative models, respectively. The qualitative model only consisted of transient calibration, and the boundary conditions were similar to the quantitative model. It should be indicated that the values assigned to the boundaries are equal to the observation wells located at or near the boundaries.

In this research, 28% of agricultural water, 65% of urban and rural drinking water, and 65% of industrial water return to the aquifer as surface recharge. Moreover, 80% of the effective rainfall causes surface recharge [47]. The initial values of the recharge rate were estimated from field data and then calibrated during the modeling. Hydraulic conductivity (K) and specific yield (Sy) were considered unknown parameters to be determined by calibration. Since these parameters change in different parts of the aquifer, the average value is first applied for each cell. Afterward, the trial-and-error method and PEST optimizer were employed for the calibration of the K and Sy values, respectively.

In this area, 6 qanats and 992 pumping wells are being used to extract water from the aquifer. There are also 27 and 23 piezometric wells to measure the water level in the steady-state and transient models, respectively. Monthly water level data for all piezometric wells were used as the observed target for calibration. Additionally, every year was divided into 4 stress periods, corresponding to one season during which the pumping rate was constant.

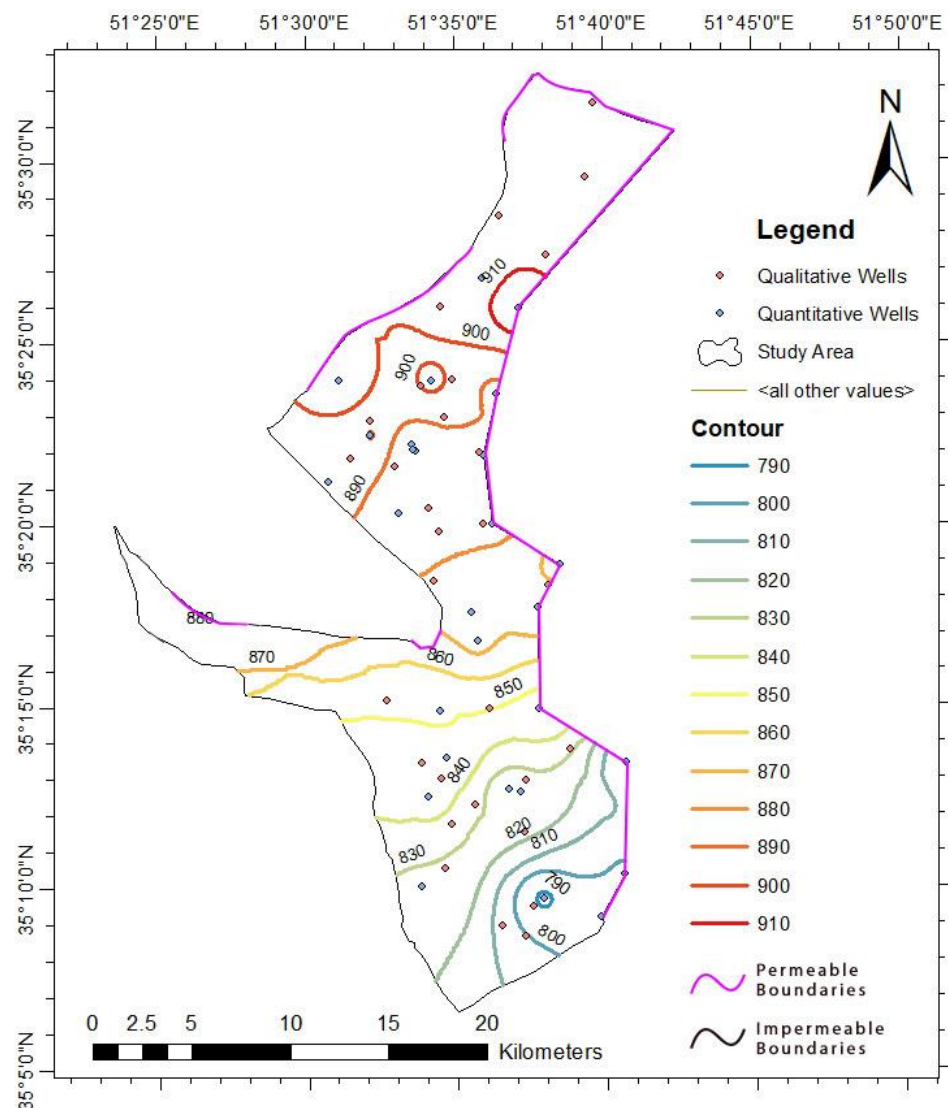


Figure 5. The permeable and impermeable boundary conditions.

2.5. Primary Information of Transport Modeling

The simulation of the solute transport was performed based on the values of hydraulic heads and flow terms calculated by MODFLOW. In this study, the concentrations of TDS, CL^- , and Na^+ ions were modeled using advection and dispersion transport packages as the main transport mechanisms.

Since the MT3DMS qualitative analysis code uses the results of the MODFLOW quantitative model, the same grids, time steps, and stress periods were selected at this stage. The boundary conditions in this solute-transport model are defined similarly to MODFLOW.

Because of the extent of the study area, determining the appropriate values for longitudinal and latitudinal dispersion coefficients is complicated. According to the field data, the value of α_L was considered as 1 m. The other coefficient α_T , which is usually expressed as a fraction of α_L ($\alpha_T/\alpha_L = 0.1$), was obtained as 0.1 m by calibration and trial-and-error [47].

The most important pollutant sources entering from the surface to the aquifer in the Varamin Plain are domestic wastewater and agricultural pollutants penetrating the soil and aquifer [47]. There exist 20 observation wells in all three models (transport of TDS, CL^- , and Na^+), which are being used to measure the concentration of the pollutants. Because of the limited field data, the monthly concentration data at all observation wells were repaired by the linear interpolation method and used as the observed target data for calibration.

2.6. Climate Change Scenarios and Downscaling

The climate projection data were provided from the GCM model of CanESM2, which is part of the Coupled Model Intercomparison Project Phase 5 (CMIP5) under the three future scenarios of RCP 2.6, 4.5, and 8.5 [21]. Because of the coarse spatial resolution of the GCM models, the statistical downscaling model of SDSM was applied to estimate the local climatic variables of temperature and precipitation. To downscale the parameters of temperature and precipitation, two synoptic stations and four rain-gauge stations were used, respectively. The properties of these stations are listed in Table 1. In this method, to derive the statistical relationship between the GCM predictors and the local predictand, the historical data used were from 1986 to 2016.

Table 1. Rain gauge and synoptic stations.

Station	Type	Altitude (m)	Latitude (Degrees)	Longitude (Degrees)
RGS-1	Rain gauge	840	35° 15' 54"	51° 34' 6"
RGS-2	Rain gauge	1000	35° 19' 45"	51° 40' 1"
RGS-3	Rain gauge	950	35° 24' 7"	51° 35' 51"
RGS-4	Rain gauge	1150	35° 30' 29"	51° 47' 2"
Sys-1	Synoptic	861	35° 12' 37"	51° 40' 4"
Sys-2	Synoptic	1299	35° 35' 53"	51° 46' 48"

2.7. Determination of ET_0 , ET_C , and IWN

Estimating the reference evapotranspiration is essential in estimating the crop water need, ET_C , and irrigation water need. In this study, the Hargreaves equation was used to calculate ET_0 , as follows [49]:

$$ET_0 = 0.0023RA(T + 17.8)TD \quad (3)$$

In which RA is the extraterrestrial radiation, T denotes the mean temperature in degrees Celsius, and TD is the difference between the maximum and minimum temperature. The value of RA is computed from [49] for each month.

To determine the crop water need, the crop coefficients, K_C , were derived from the Food and Agriculture Organization (FAO), and the following formula was used [50]:

$$ET_C = K_C ET_0 \quad (4)$$

In the last step, the irrigation water need was determined from the difference of the ET_C and the effective precipitation, P_e , as follows [50]:

$$IWN = ET_C - P_e \quad (5)$$

3. Result

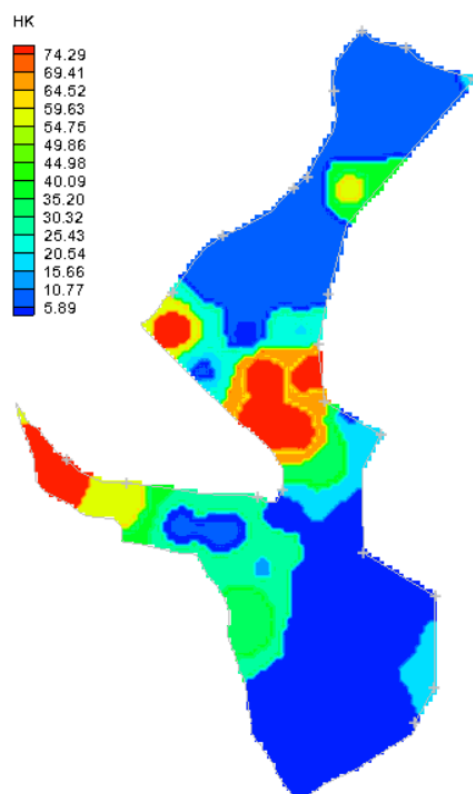
3.1. MODFLOW Calibration and Validation Results

The model's calibration was conducted in two stages, including the steady-state and transient analyses. For the calibration of the steady-state condition, the parameters of the hydraulic conductivity and recharge rate were estimated at the beginning of the adjustment period, March 2008, as listed in Table 2. Then, the transient MODFLOW model was calibrated for the two parameters of recharge rate and specific yield of the aquifer (S_y) using monthly observed water levels from March 2016 (Table 2). The measured data for the two next years (2017 and 2018) were used during the validation stage. The initial conditions of the aquifer to implement the model were the same groundwater level at the beginning of the analysis in March 2008.

Table 2. The calibrated parameters for the quantitative and qualitative models.

Model	Quantitative Model	Qualitative Model
Steady-state	Hydraulic conductivity, recharge	-
Transient	Recharge, specific yield	longitudinal dispersion coefficient, pollutant concentration sources

By calibration of the steady-state model, acceptable amounts of hydraulic conductivity and the recharge rate were obtained, which are presented in Figures 6 and 7. Based on the simulation results, the values of the hydraulic conductivity and recharge rate varied between 6 and 74 m/day and 0.0002 and 0.004 m/day, respectively. It should be indicated that in [41], the hydraulic conductivity in the western Varamin Plain was in the same range. Figure 8 illustrates the correlation between the observed and calculated water level values in the piezometric wells of the aquifer for March 2008. The correlation was very high ($R^2 = 0.99$) and indicates the high adaptation of the model in the steady-state flow. Also, the groundwater level resulting from the numerical model is shown in Figure 9. The computed groundwater level varied between 776 and 966 m.

**Figure 6.** Distribution of the calibrated values of the hydraulic conductivity parameter in the plain during the steady-state calibration.

During the transient model's calibration, an acceptable amount of specific yield was calibrated. Based on the simulation results, the values of the specific yield varied between 2 and 33%. In [41], the specific yield for the unconfined aquifer was between 3 and 20%, which is similar to the results obtained in this study. To compare the results, the correlation between the observed and modeled water level values for the calibration period was computed, which equaled 0.9937 (Figure 10). Also, the variations in the simulated groundwater levels from 2008 to 2016 are shown in Figure 11. For the validation process, the correlation between the observed and modeled water level values is shown in Figure 12, which yielded the R^2 value of 0.9918.

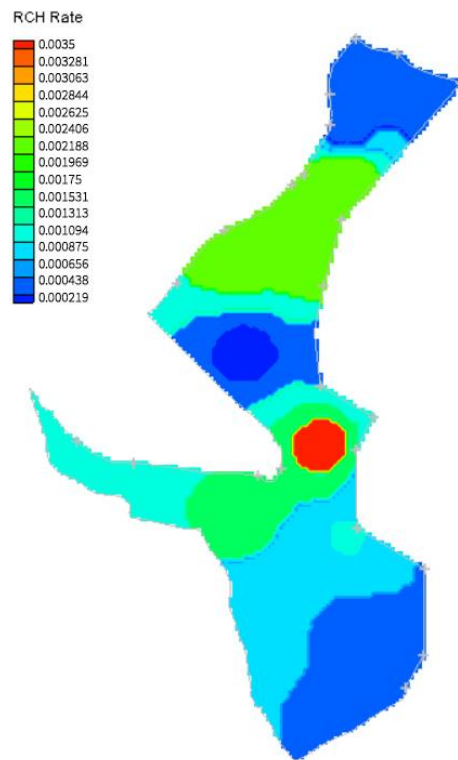


Figure 7. Distribution of the calibrated values of the recharge rate parameter in the aquifer during the steady-state calibration (March 2008).

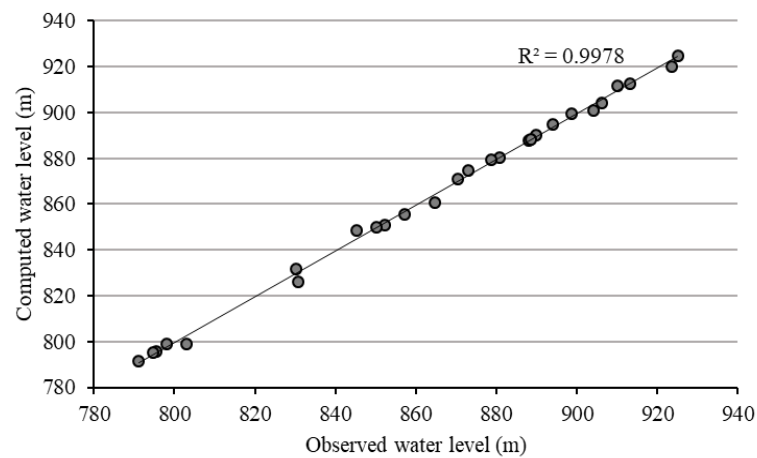


Figure 8. Correlation between the observed and computed values of the water level in the piezometric wells of the study area in the steady flow (March 2008).

The results in the calibration and validation phases ensure the high accuracy of the model. Moreover, to investigate the outcomes, error-based measures, including ME (mean error), MAE (mean absolute error), RMSE (root mean square error), and MRE (mean relative error), are presented in Table 3. These measures are given in the following forms in Equations (6)–(9) [51]:

$$ME = \frac{1}{n} \left(\sum_{i=1}^n O_i - S_i \right) \tag{6}$$

$$MAE = \frac{1}{n} \left(\sum_{i=1}^n |O_i - S_i| \right) \tag{7}$$

$$RMSE = \sqrt{\frac{1}{n} \sum_{i=1}^n (O_i - S_i)^2} \tag{8}$$

$$MRE = \frac{RMSE}{\Delta} \tag{9}$$

where O_i and S_i are the measured and simulated parameters at observation well i , respectively. In the definition of the MRE, Δ equals the difference between the maximum and minimum observed values [51].

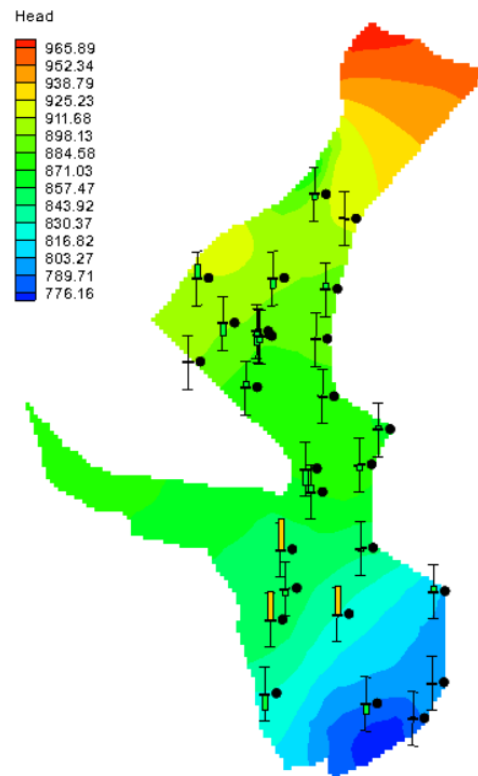


Figure 9. Groundwater level in the Varamin aquifer in the steady flow (March 2008) (Black circles represent quantitative wells).

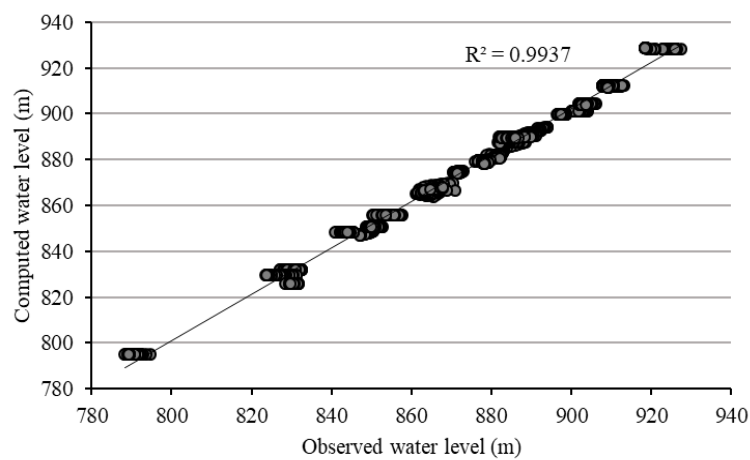


Figure 10. Correlation between the observed and computed values of the water level in the piezometer wells of the Varamin aquifer in the transient flow (2008–2016).

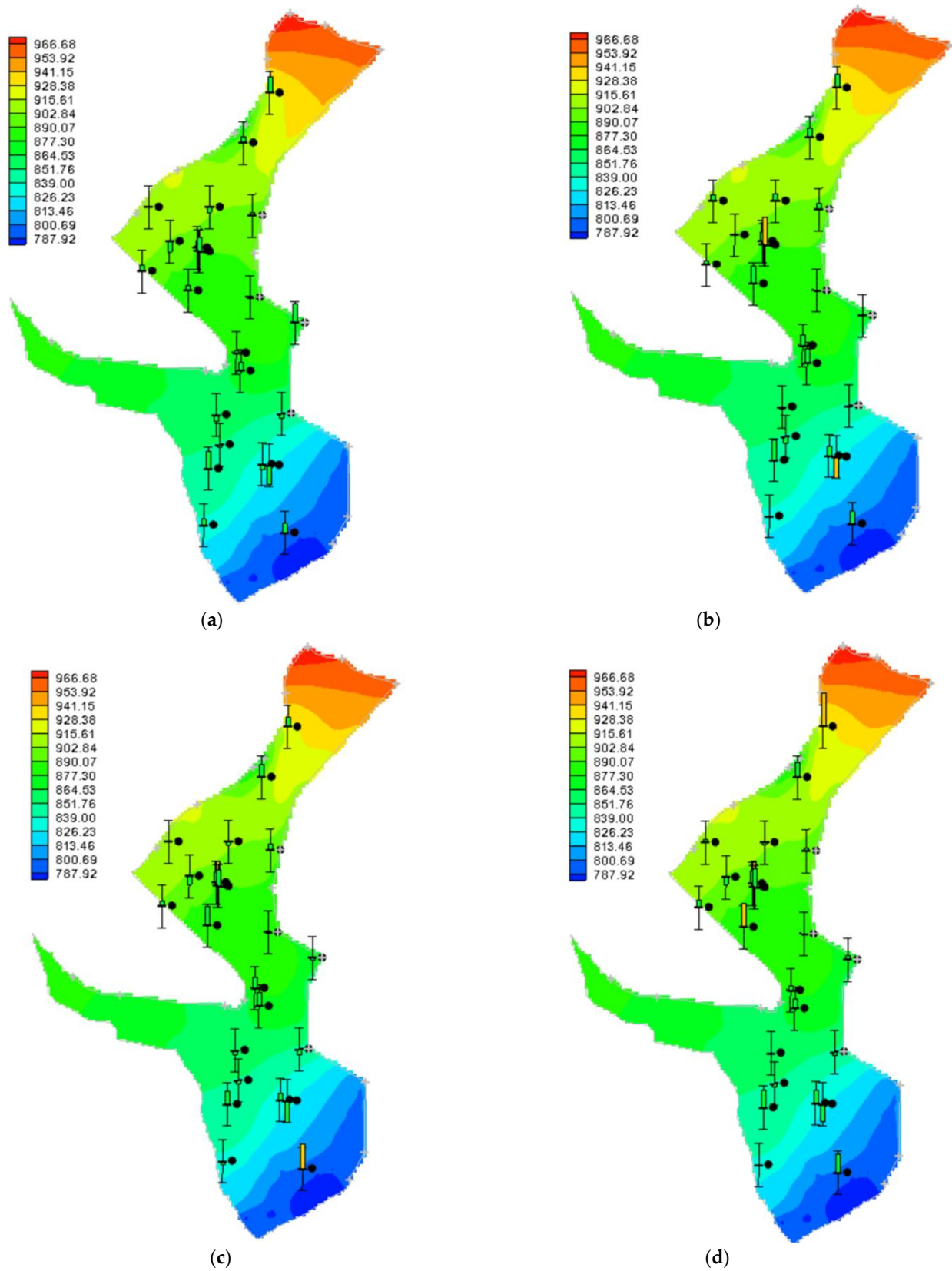


Figure 11. Groundwater level in the Varamin aquifer in the transient flow: (a) 2008; (b) 2010; (c) 2012; (d) 2014 (Black circles represent quantitative wells).

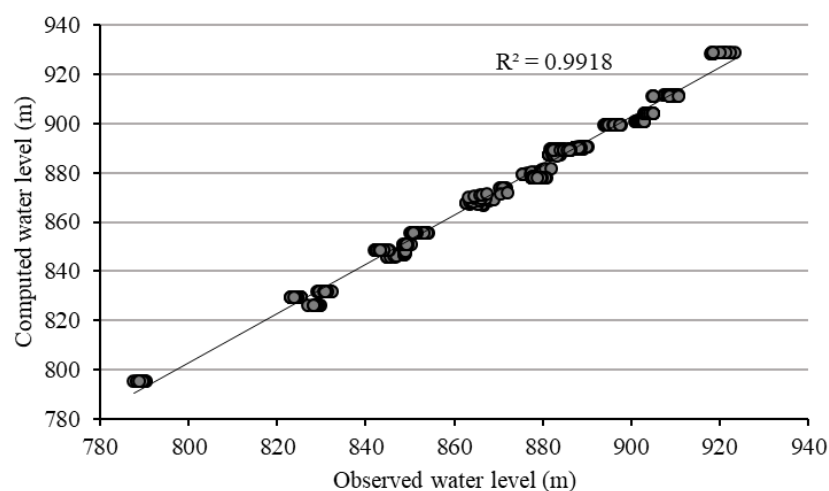


Figure 12. Correlation between the observed and computed values of the water level in the piezometer wells of the Varamin aquifer during the validation process (2016–2018).

Table 3. Calculated errors of the quantitative model.

Models	ME (m)	MAE (m)	RMSE (m)	MRE (%)
Calibration (steady state)	−0.51	1.44	1.99	1.48
Calibration (transient)	1.98	2.6	3.25	2.34
Validation	2.14	2.74	3.42	2.52

The sensitivity analysis was performed for the three calibrated parameters of hydraulic conductivity, specific yield, and recharge. For the two parameters of specific yield and recharge, the results are listed in Table 4. The minimum value of 2% and 0.0002 m/day was assumed for the specific yield and recharge rate, respectively. Therefore, for the calculation of the RMSE, an increase in the value of these parameters up to 30% was assumed.

Table 4. Calculated errors for the increase in the calibrated parameters of the recharge rate and specific yield.

Calibrated Parameter	0%	+10%	+20%	+30%
Recharge rate	3.25	3.252	3.254	3.256
Specific yield	3.25	3.256	3.261	3.266

Moreover, for the hydraulic conductivity the maximum value of 80 m/day was considered in the study area according to the field data and previous studies. Hence, a decrease up to 30% was considered to compute the RMSE values as presented in Table 5.

Table 5. Calculated errors for the increase in the calibrated parameter of hydraulic conductivity.

Calibrated Parameter	0%	−10%	−20%	−30%
Hydraulic conductivity	3.25	3.252	3.254	3.256

3.2. MT3D Calibration and Validation Results

In the next step, first, the contaminants' concentration was entered in different periods of the qualitative model in the transient state. Second, the longitudinal dispersion coefficient and pollutants concentration sources were calibrated using data from March 2008 to March

2016, and an acceptable tolerance was obtained. Finally, the qualitative model was validated against the data from the wells from March 2016 to March 2018. Consequently, as presented in Table 6, the calculated errors derived by comparing each pollutant's modeled and observed concentrations for both the calibration and validation periods in this area were reasonable. It should be mentioned that the concentration of the parameters, including TDS, chloride, and sodium, in March 2008 was assumed as the initial condition.

Table 6. Calculated errors of qualitative models.

Models	ME (mg/L)	MAE (mg/L)	RMSE (mg/L)	MRE (%)
TDS—calibration	3.5	277.97	432.72	7.78
CL [−] —calibration	−0.49	3.4	5.77	9.4
Na ⁺ —calibration	0.23	2.58	4.16	9.27
TDS—validation	23.51	273.46	416.49	9.4
CL [−] —validation	−0.58	3.51	5.87	10.09
Na ⁺ —validation	0.74	2.83	4.33	8.7

3.2.1. TDS

In this section, Figure 13 illustrates the correlation between the observed and modeled TDS concentration values from March 2008 to March 2016. Accordingly, the high correlation value of 0.93 indicates a suitable modification of the solute-transport model. Also, the changes in the calculated concentration of TDS from 2008 to 2016 are shown in Figure 14.

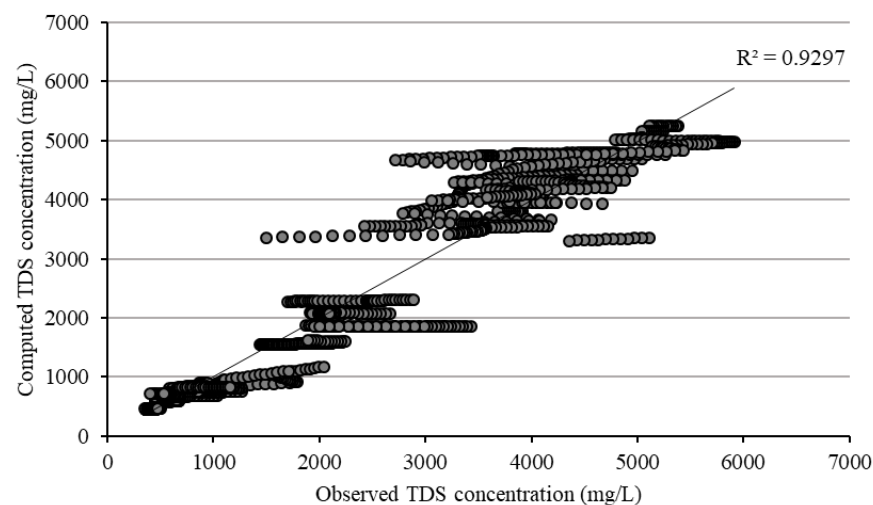


Figure 13. Correlation between the observed and computed values of the TDS concentration in the observation wells of the Varamin aquifer in the transport modeling (2008–2016).

Figure 15 illustrates the correlation between the observed and modeled TDS concentration values for the validation period. Accordingly, the high correlation value of 0.95 indicates an acceptable adaptation of the model during the validation process. Also, the latest change in the calculated concentration of TDS from 2016 to 2018 is shown in Figure 16.

3.2.2. Chloride

Figure 17 illustrates the correlation between the observed and modeled Cl[−] concentration values from March 2008 to March 2016 in which R² was equal to 0.8522. Also, the changes in the calculated concentration of Cl[−] from 2008 to 2016 are shown in Figure 18. In Figure 19, the correlation between the measured and simulated values of Cl[−] is depicted during the validation stage, and the R² value of 0.83 is computed. The spatial distribution of Cl[−] from 2016 to 2018 is shown in Figure 20.

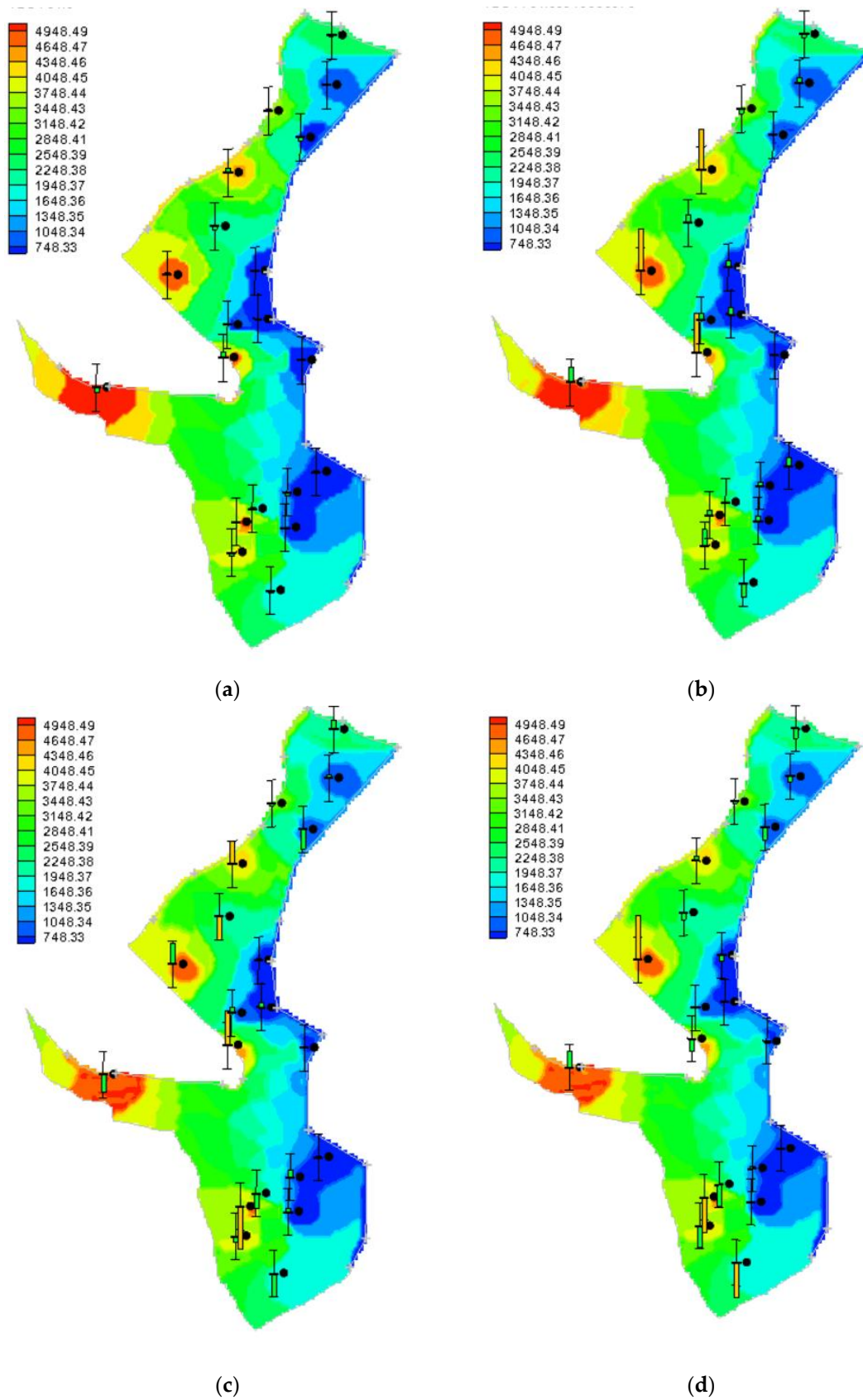


Figure 14. TDS concentration in the Varamin aquifer in the transport modeling: (a) 2008; (b) 2010; (c) 2012; (d) 2014 (Black circles represent qualitative wells).

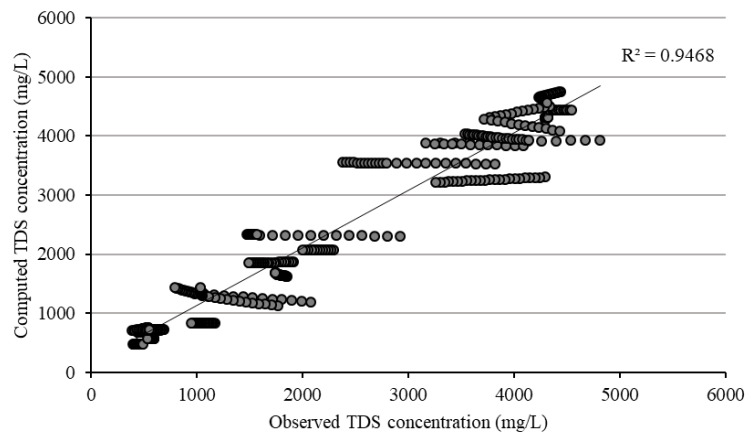


Figure 15. Correlation between the observed and computed values of the TDS concentration in the observation wells of the Varamin aquifer during the validation process (2016–2018).

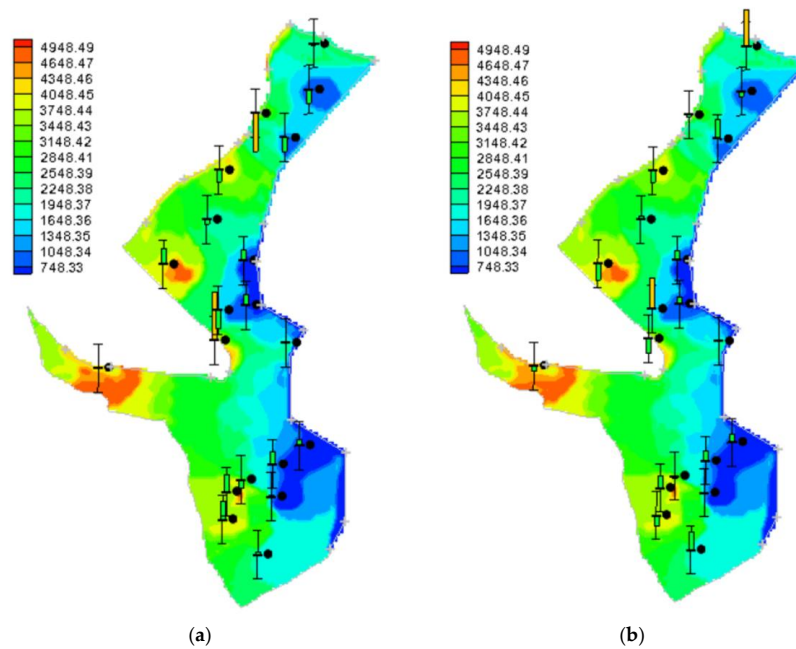


Figure 16. TDS concentration in the Varamin aquifer during the validation process: (a) 2016; (b) 2018 (Black circles represent qualitative wells).

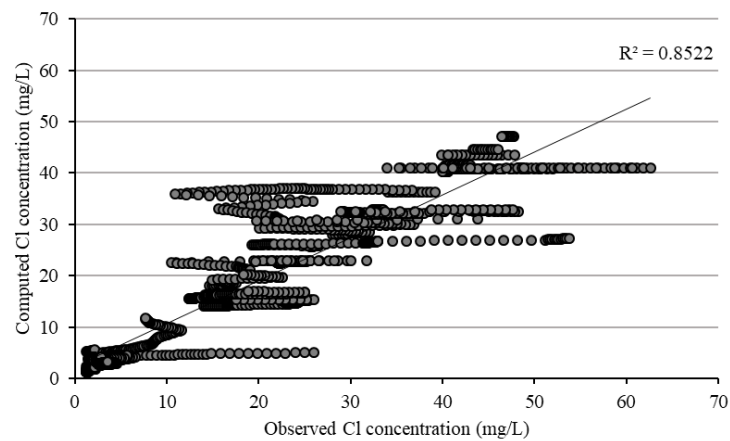


Figure 17. Correlation between the observed and computed values of the Cl^- concentration in the observation wells of the Varamin aquifer in the transport modeling (2008–2016).

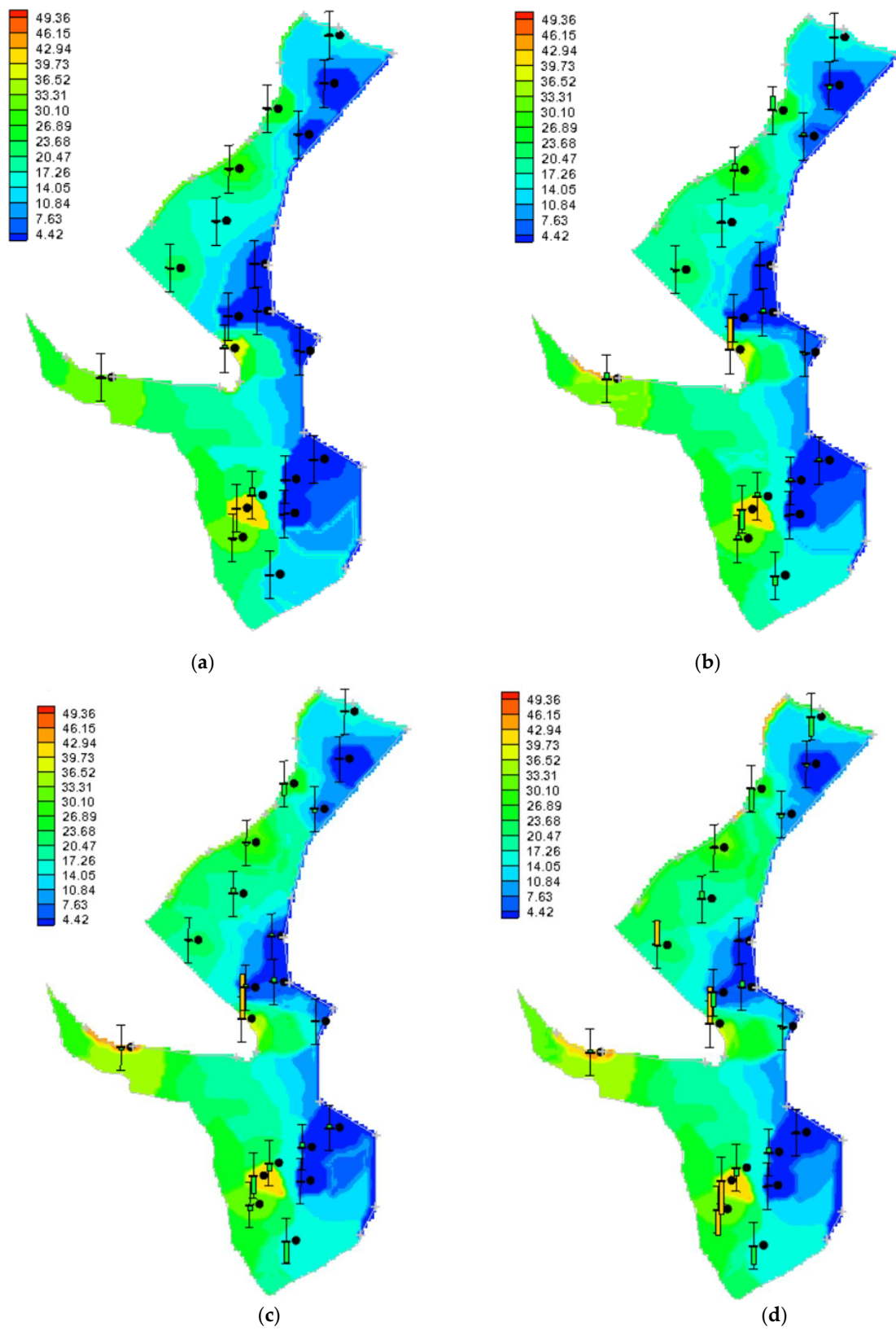


Figure 18. Cl^- concentration in the Varamin aquifer in the transport modeling: (a) 2008; (b) 2010; (c) 2012; (d) 2014 (Black circles represent qualitative wells).

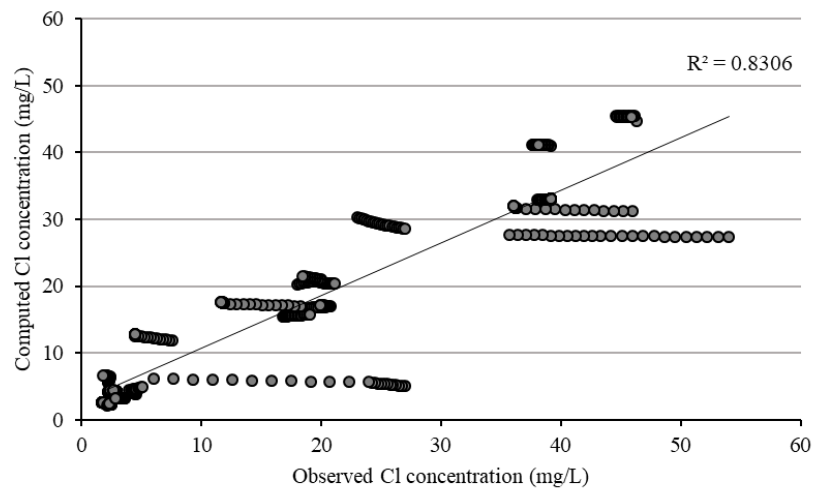


Figure 19. Correlation between the observed and computed values of the Cl^- concentration in the observation wells of the Varamin aquifer during the validation process (2016–2018).

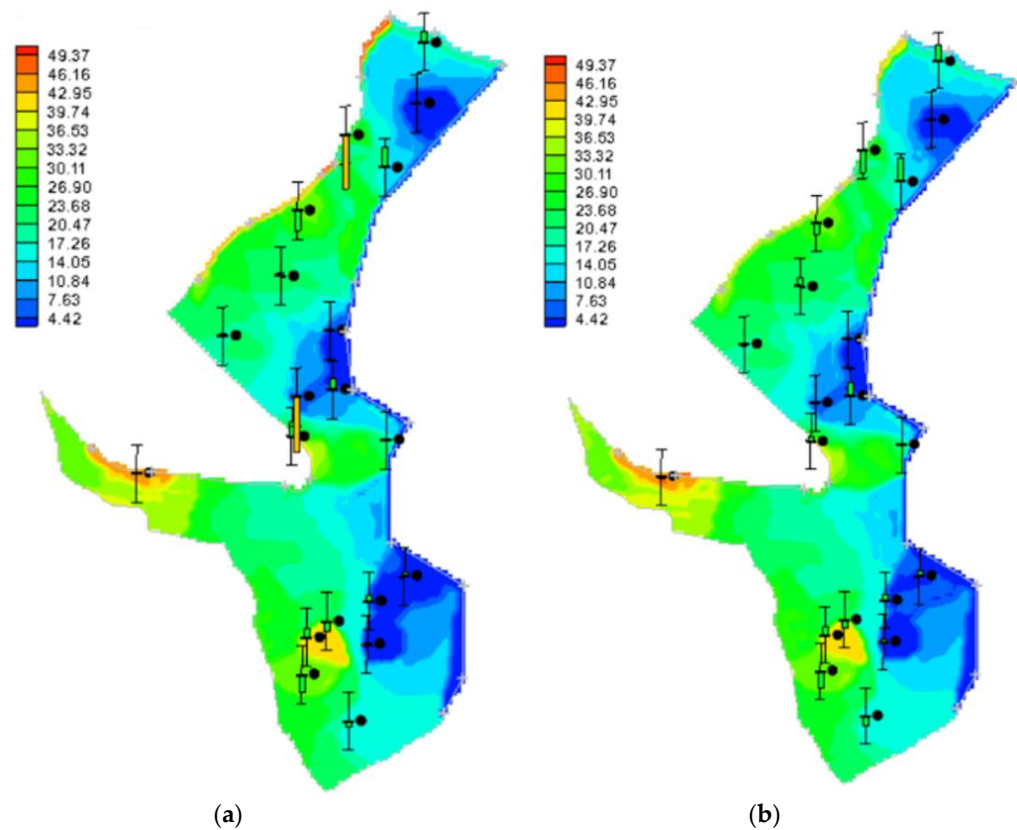


Figure 20. Cl^- concentration in the Varamin aquifer during the validation process: (a) 2016; (b) 2018 (Black circles represent qualitative wells).

3.2.3. Sodium Ion

The correlation between the observed and calculated Na^+ concentration values for the calibration is shown in Figure 21. Moreover, the maps of the Na^+ concentration during the calibration period is displayed in Figure 22. For the validation period, the results are presented in Figures 23 and 24, respectively. The high values of the correlations in the Figures 21 and 23, suggest a very good agreement between the measured and simulated data.

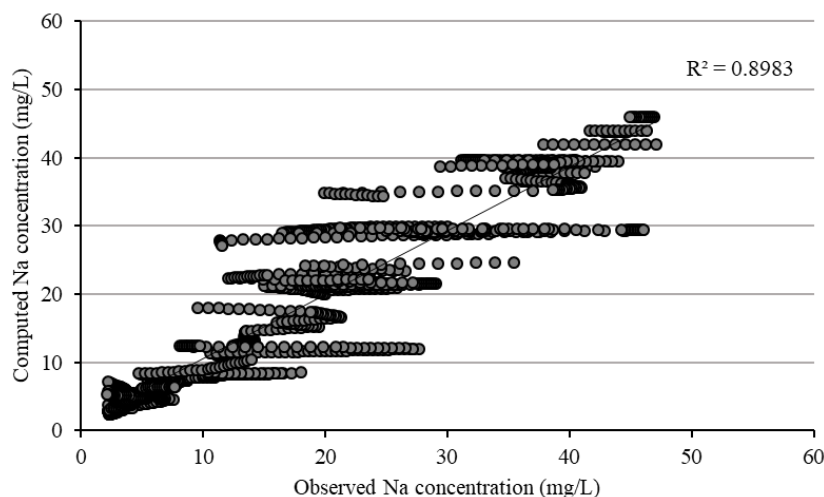


Figure 21. Correlation between the observed and computed values of the Na⁺ concentration in the observation wells of the Varamin aquifer in the transport modeling (2008–2016).

3.3. SDSM Calibration, Validation, and Prediction Results

In this stage, to calibrate the SDSM model, different sets of predictors were screened for a period of twenty years (1986–2006) at each station. The list of screened variables is presented in Tables 7 and 8. It should be indicated that the National Centre for Environmental Prediction (NCEP) re-analysis data set was used for the model calibration. In the next step, to verify the model, observed and generated results were compared from 2006 to 2016 (Figures 25 and 26). As illustrated in these figures, a good agreement exists between the downscaled and observed data.

Table 7. The selected predictors for the downscaling of the precipitation for each rain gauge station.

Station	Selected Predictors
RGS-1	Zonal velocity component near the surface (p_u) Meridional velocity component at 500 hPa (p5_v) 500 hPa geopotential height (p500) Divergence at 500 hPa (p5zh) Total precipitation (prec) Near surface specific humidity (shum) Near surface air temperature (temp)
RGS-2	Vorticity at 500 hPa (p5_z) 500 hPa geopotential height (p500) Vorticity at 850 hPa (p8_z) 850 hPa geopotential height (p850) Total precipitation (prec) Near surface specific humidity (shum)
RGS-3	Vorticity at 500 hPa (p5_z) 500 hPa geopotential height (p500) Vorticity at 850 hPa (p8_z) 850 hPa geopotential height (p850) Total precipitation (prec) Near surface specific humidity (shum)
RGS-4	Meridional velocity component at 500 hPa (p5_v) 500 hPa geopotential height (p500) Vorticity at 850 hPa (p8_z) 850 hPa geopotential height (p850) Total precipitation (prec) Near surface specific humidity (shum) Near surface air temperature (temp)

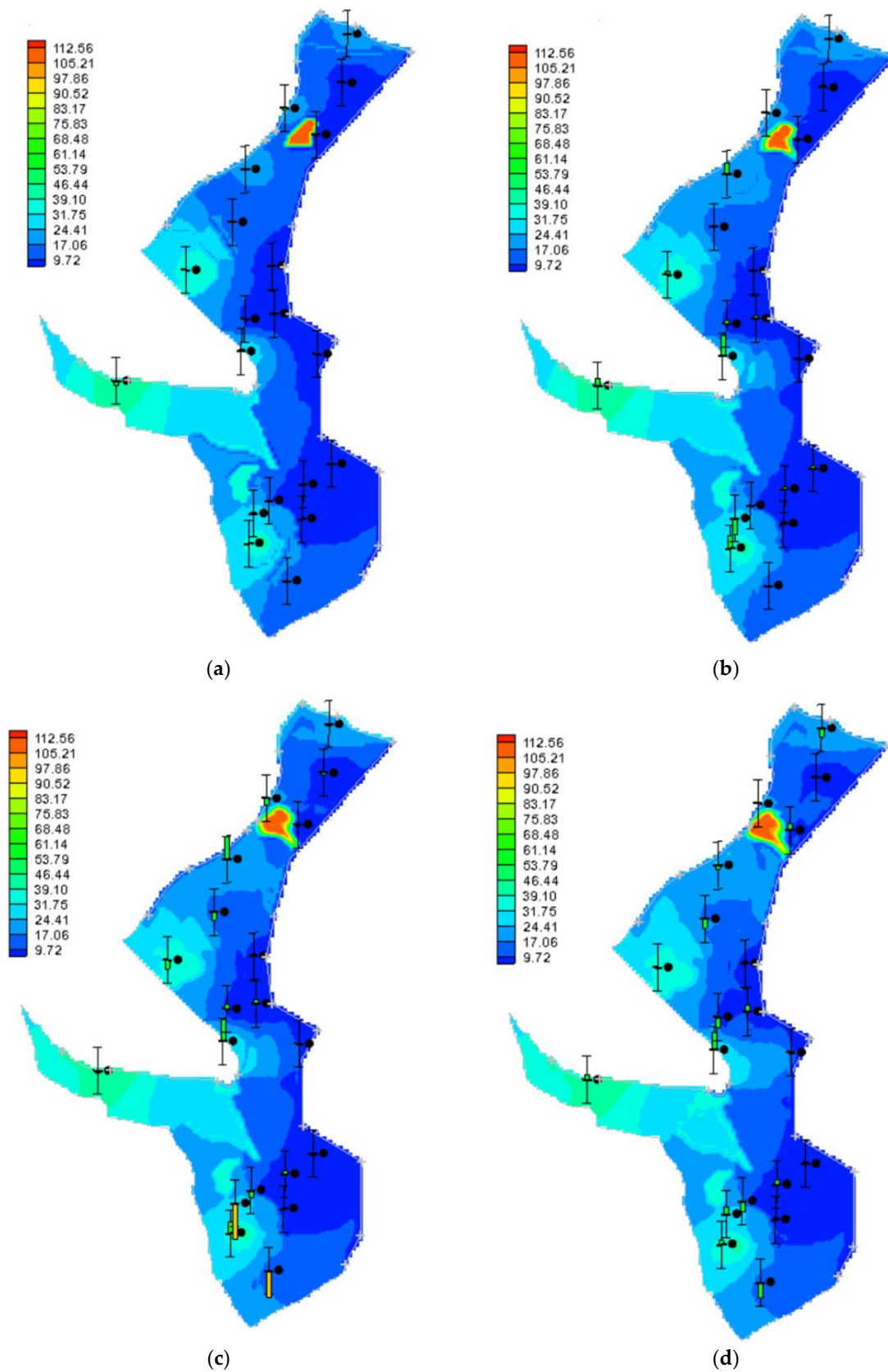


Figure 22. Na^+ concentration in the Varamin aquifer in the transport modeling: (a) 2008; (b) 2010; (c) 2012; (d) 2014 (Black circles represent qualitative wells).

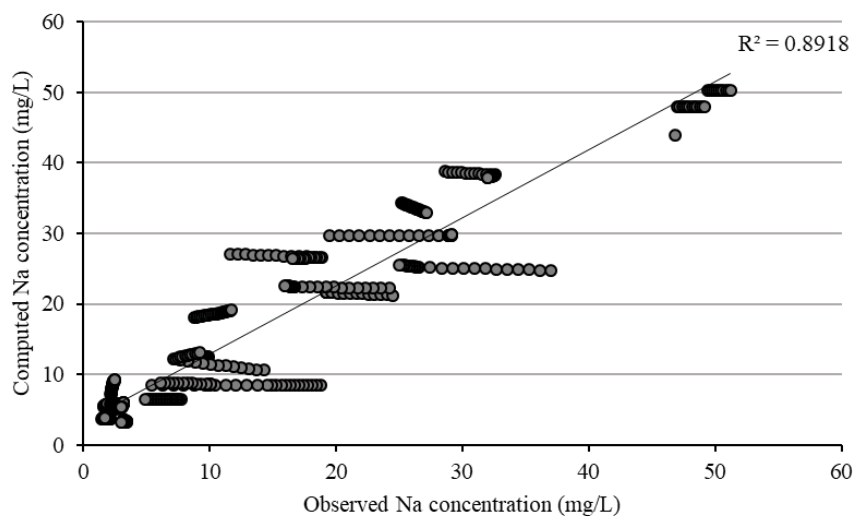


Figure 23. Correlation between the observed and computed values of the Na⁺ concentration in the observation wells of the Varamin aquifer during the validation process (2016–2018).

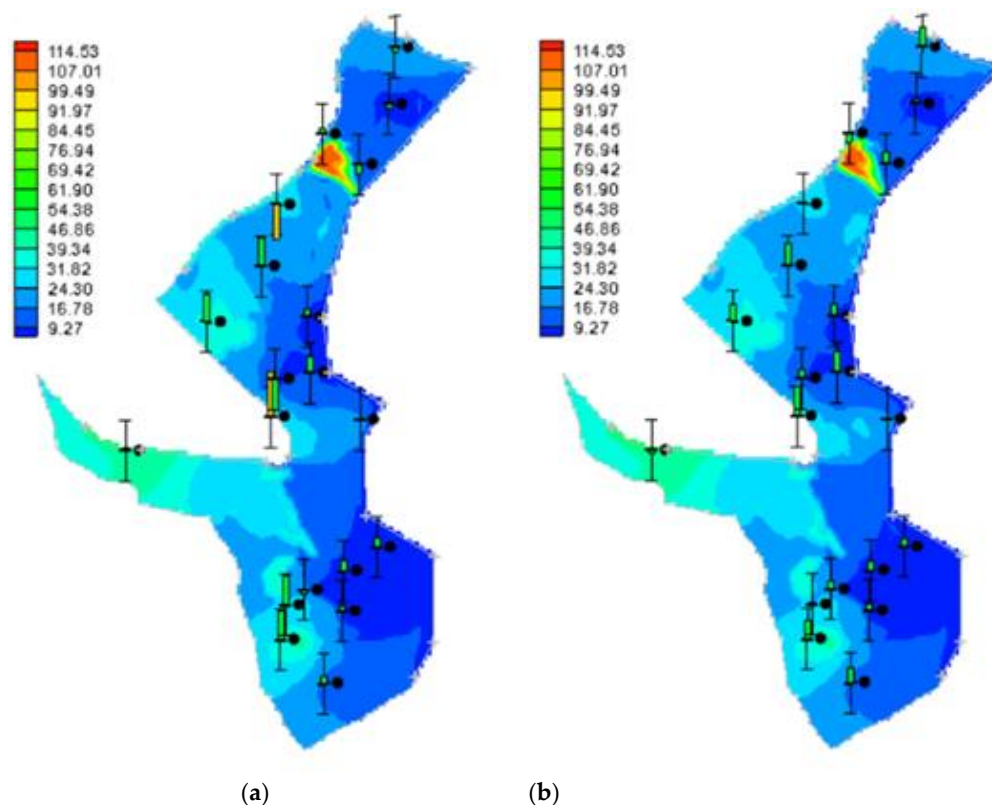


Figure 24. Na⁺ concentration in the Varamin aquifer during the validation process: (a) 2016; (b) 2018 (Black circles represent qualitative wells).

Table 8. The selected predictors for the downscaling of temperature for each synoptic station.

Station	Selected Predictors
SyS-1	500 hPa geopotential height (p500) Near surface air temperature (temp)
SyS-2	500 hPa geopotential height (p500) Near surface air temperature (temp)

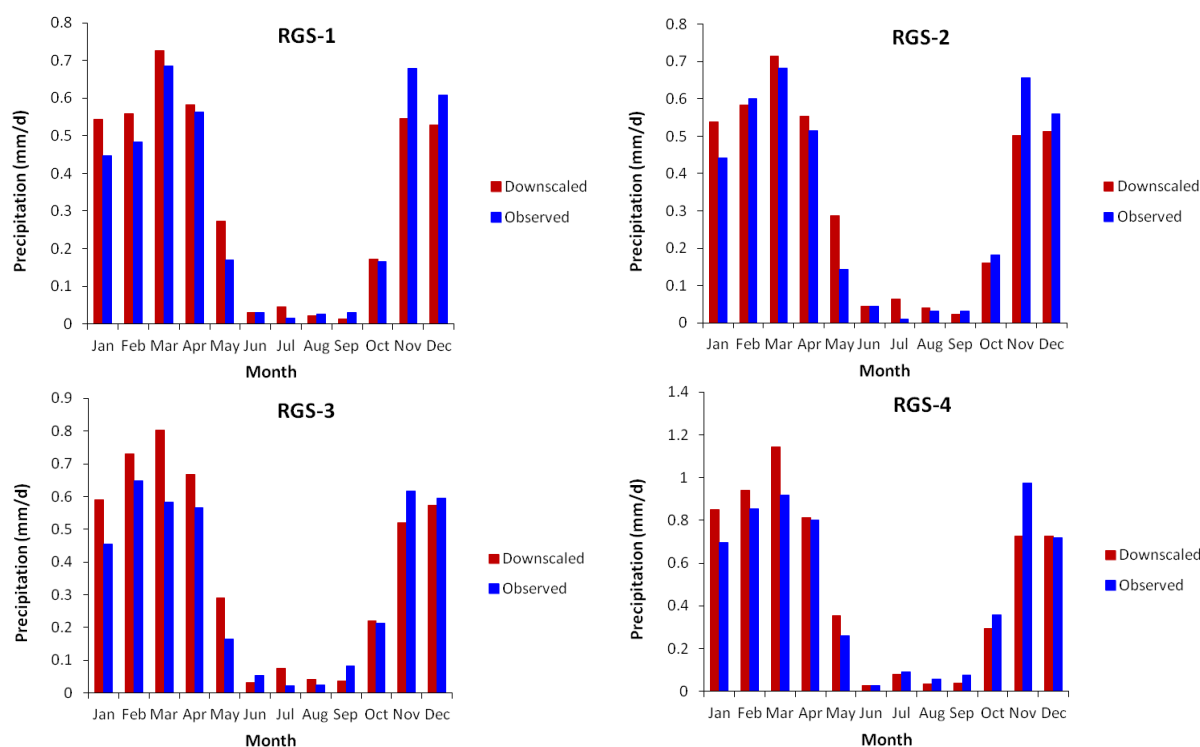


Figure 25. The comparison between the downscaled (using NCEP predictors) and observed precipitation for the period of 2006–2016 at the different rain gauge stations.

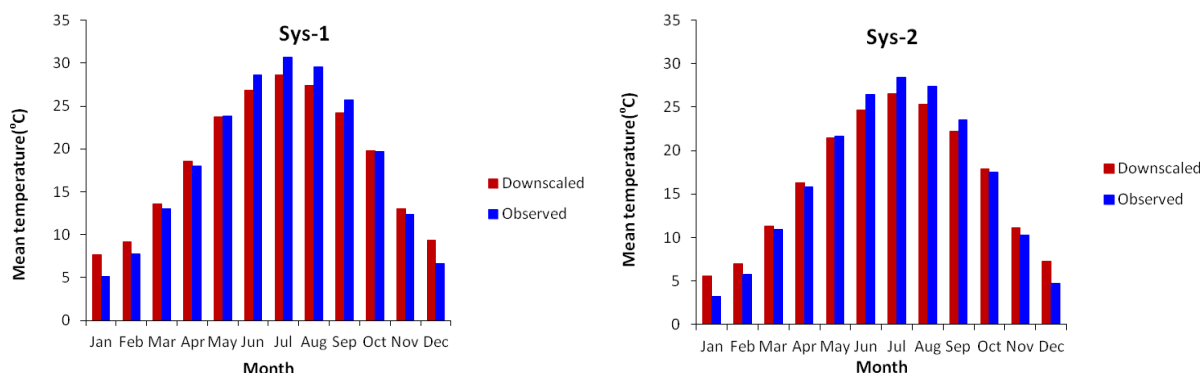


Figure 26. The comparison between the downscaled (using NCEP predictors) and observed daily mean temperature for the period of 2006–2016 at the different synoptic stations.

After the evaluation of the downscaling models, the synthetic daily weather series was generated for the time period of 2025–2054 at different stations with the GCM predictors. The annual mean values under the three scenarios of RCP2.6, RCP4.5, and RCP8.5 for the two parameters of precipitation and mean temperature are shown in Figure 27. From these figures, the following observations are made: (1) the annual mean precipitation decreased between 0.02 and 0.34 mm/day for the different rain gauge stations under the three emission scenarios; (2) the annual mean temperature is expected to increase between 1.94 and 2.57 degrees; and (3) the increases in temperature are the most severe with RCP 8.5, while RCP 4.5 shows the largest reduction in precipitation.

3.4. Climate Change Effect on ET_0 , ET_C , and IWN

In Figure 28, the values of ET_0 for each month were computed based on the monthly mean average temperature during the historical interval (1986–2016) and future period (2025–2055) for each RCP. Also, as mentioned above, since the major crops in the Varamin Plain include wheat, barley, corn, and alfalfa, the crop water need and irrigation water

need for each product were estimated for the historical and future emission scenarios (Figures 29 and 30). As illustrated in these figures, because of the increase in the reference evapotranspiration and decrease in the precipitation during the crop growth stage, the values of ET_C and IWN increase for the future period.

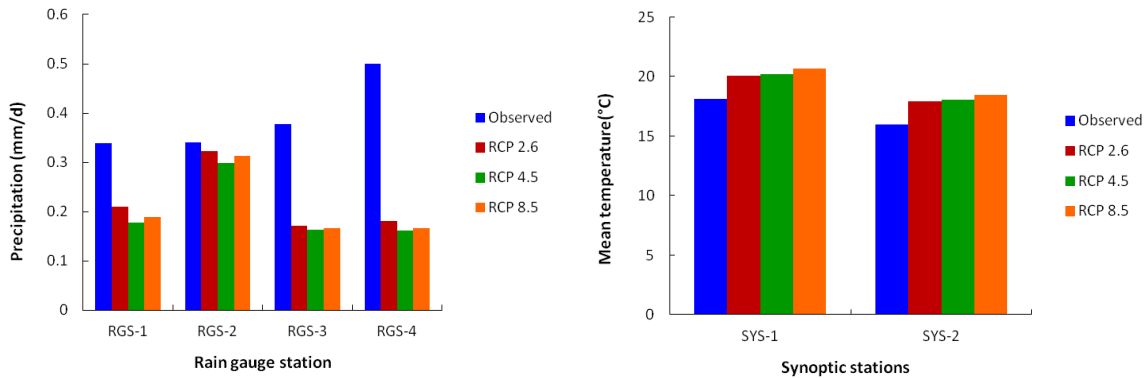


Figure 27. The annual mean values under three scenarios of RCP2.6, RCP4.5, and RCP8.5 for the two parameters of precipitation (Left) and mean temperature (Right).

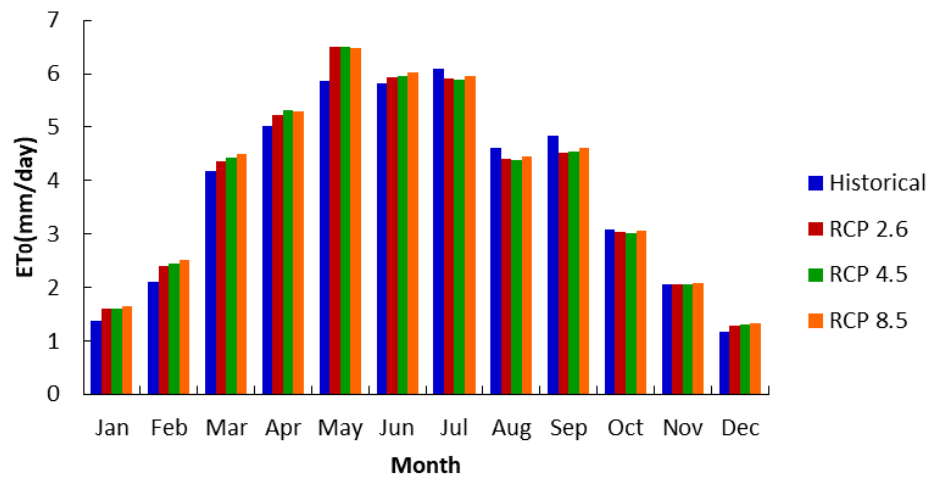


Figure 28. The values of ET_0 for each month during the historical interval and under the three scenarios of RCP2.6, RCP4.5, and RCP8.5.

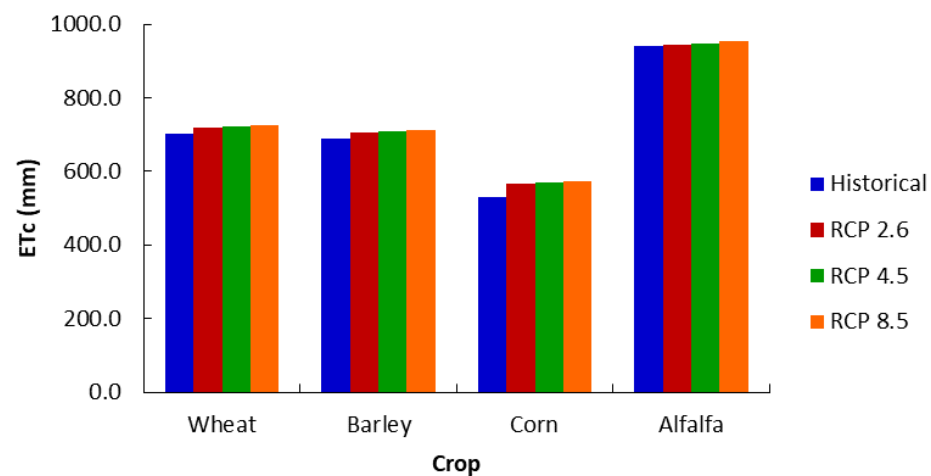


Figure 29. The values of ET_C for each crop during the historical interval and under the three scenarios of RCP2.6, RCP4.5, and RCP8.5.

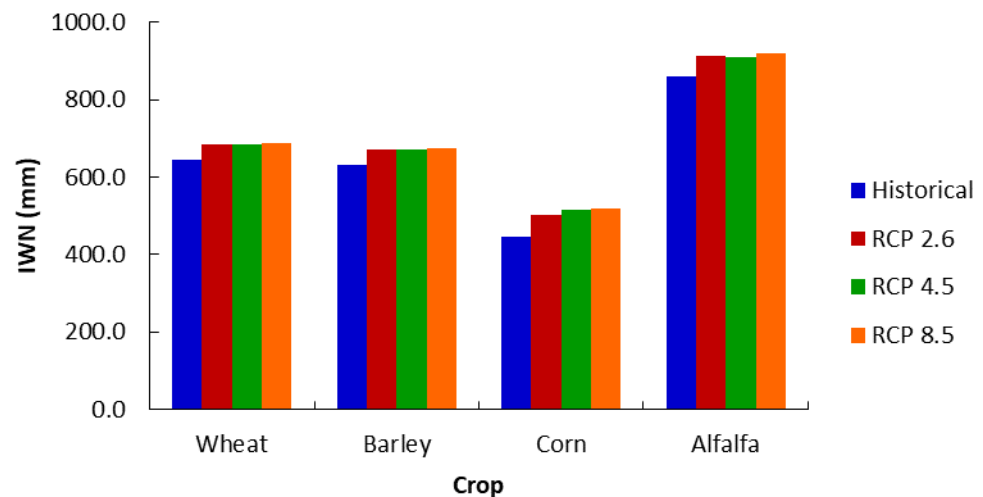


Figure 30. The values of IWN for each crop during the historical interval and under the three scenarios of RCP2.6, RCP4.5, and RCP8.5.

3.5. Predicting the Aquifer's Status in the Future

In this section, the quantitative and qualitative status of the model were predicted in light of anthropogenic and climate change effects. The prediction period was set to be 2025 to 2055. However, some parameters, such as hydraulic conductivity, specific yield, porosity, and longitudinal and latitudinal dispersion coefficients, were considered equal to the historical period (2008–2018).

3.5.1. Scenario 0: Continuing the Existing Conditions

In the first step, to compare the results, the model was implemented without considering any human or climate effects, and all parameters for the observation period were fixed for 2025 to 2055. The results indicate that in this case, the groundwater level will decline by 2.4 m, the chloride concentration will increase by 6.8 milligrams per liter, the sodium concentration will increase by 4.8 milligrams per liter, and the TDS concentration will decline by 143.2 milligrams per liter. Figures 31–34 show the groundwater level, TDS, Cl^- , and Na^+ ions concentration changes in 2025, 2035, 2045, and 2055 in the Varamin aquifer, respectively.

3.5.2. Scenario 1: Increase in the Extraction from Pumping Wells (25%)

In this scenario, the amount of extraction from pumping wells increased up to 25%, 15% of which returns to the aquifer as surface recharge. This increase in extraction can be due to the increase in drinking water demand or in agricultural and industrial activities. Under this scenario, the groundwater level will decline by 2.5 m; for the pollutants' concentration, the chloride concentration will increase by 7 milligrams per liter, the sodium concentration will increase by 5 milligrams per liter, and the TDS concentration will decline by 153.7 milligrams per liter.

3.5.3. Scenario 2: Climate Changes

The climate change effect as considered in Scenario 2. In this area, an irrigation efficiency of 60% was assumed, 15% of which returns to the aquifer as a return flow. In addition, 80% of the effective rainfall feeds the aquifer. It is obvious that under the scenarios caused by climate change, we will see more groundwater declination in comparison to Scenario 0. Furthermore, the climatic change effects on the quality of the aquifer are very insignificant.

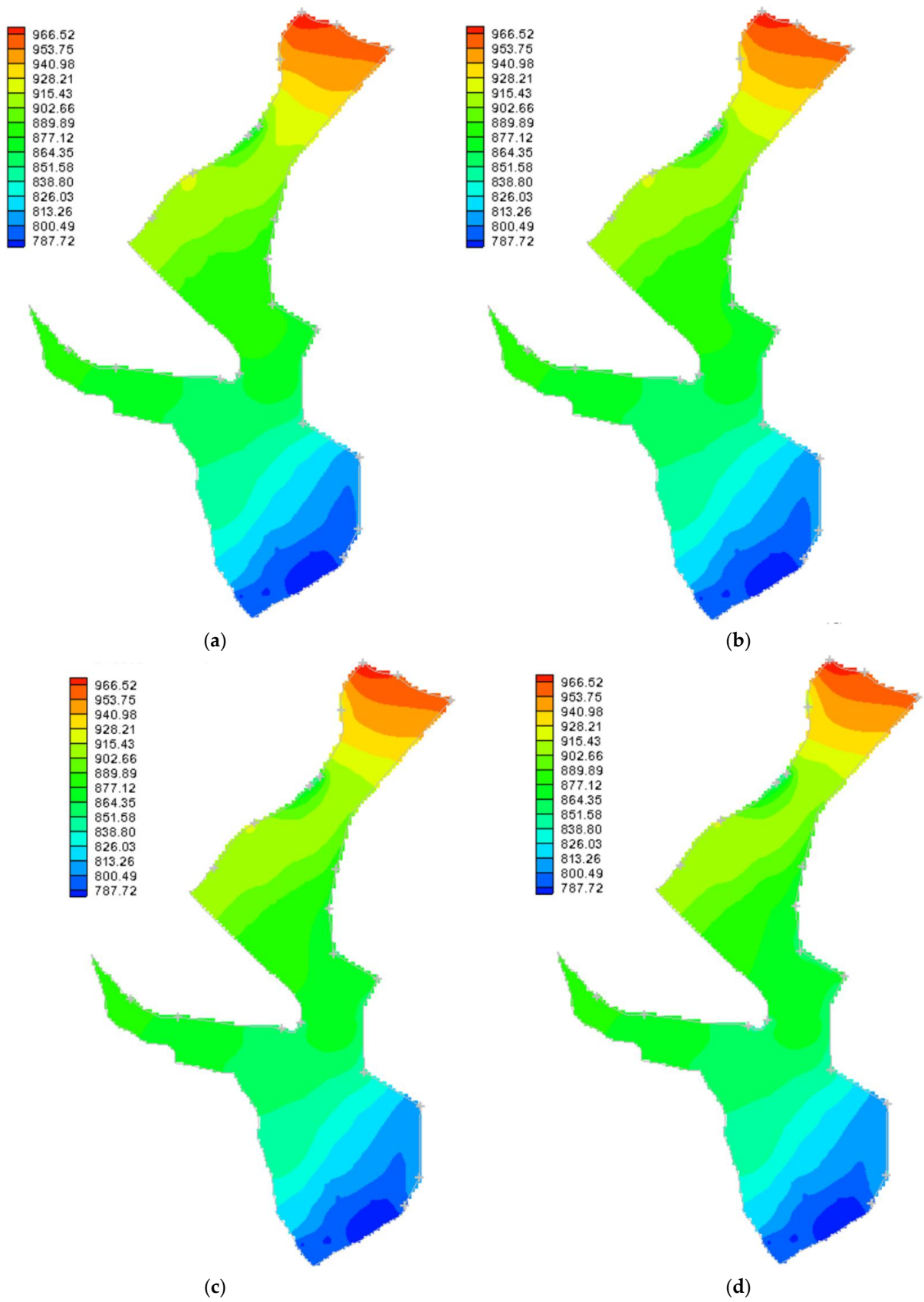


Figure 31. Groundwater level in the Varamin aquifer: (a) 2025; (b) 2035; (c) 2045; (d) 2055.

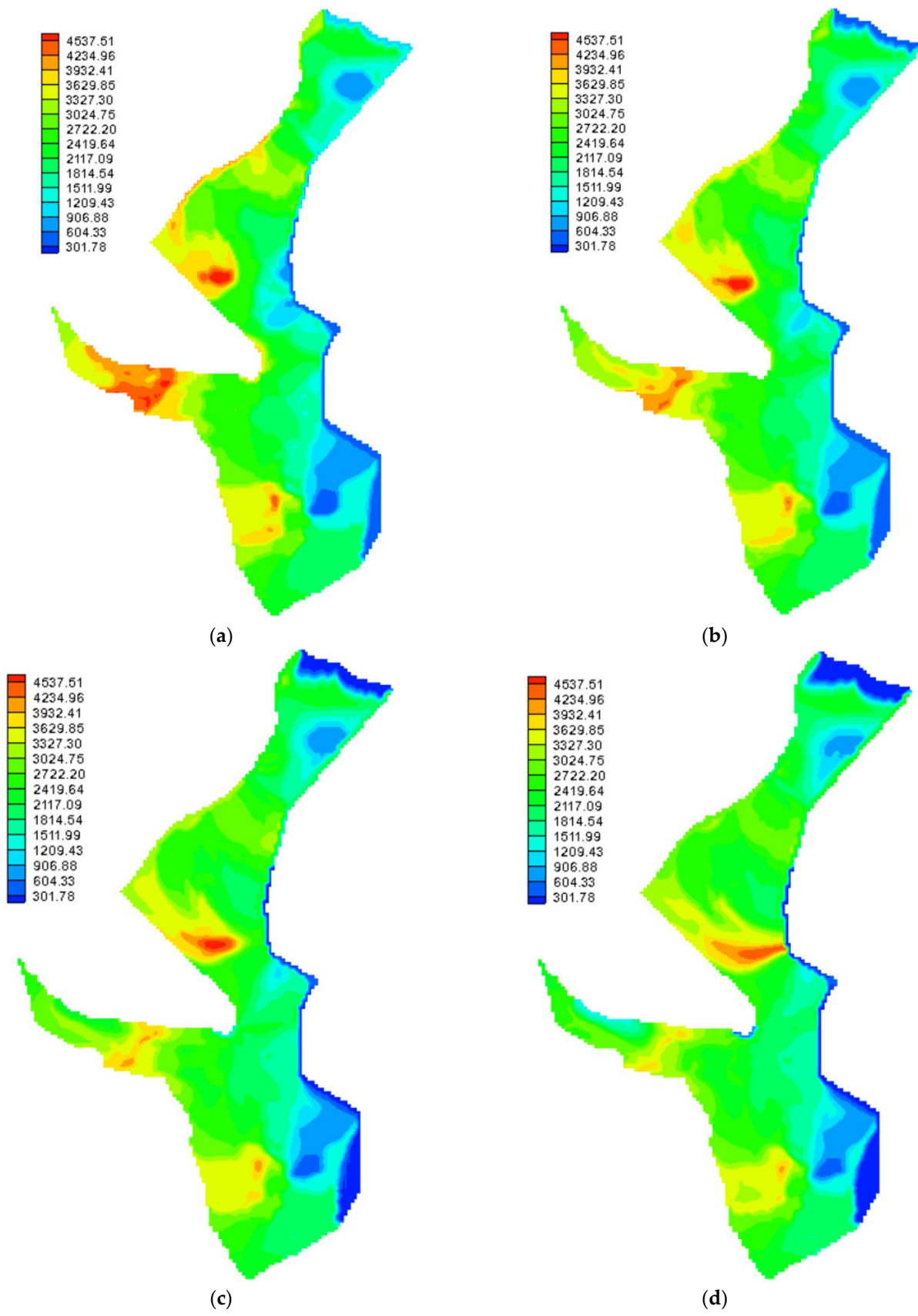


Figure 32. TDS concentration in the Varamin aquifer: (a) 2025; (b) 2035; (c) 2045; (d) 2055.

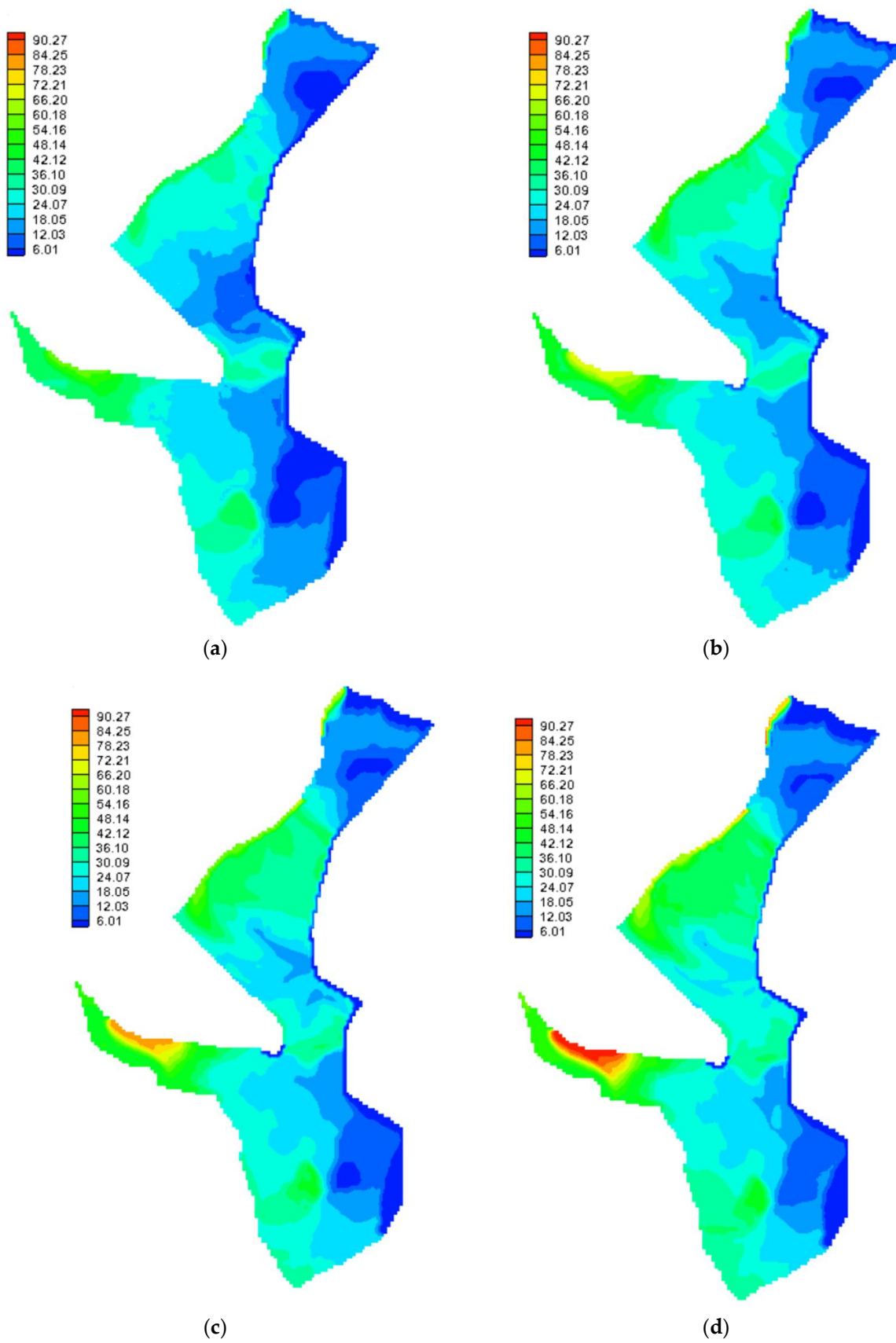


Figure 33. Chloride concentration in the Varamin aquifer: (a) 2025; (b) 2035; (c) 2045; (d) 2055.

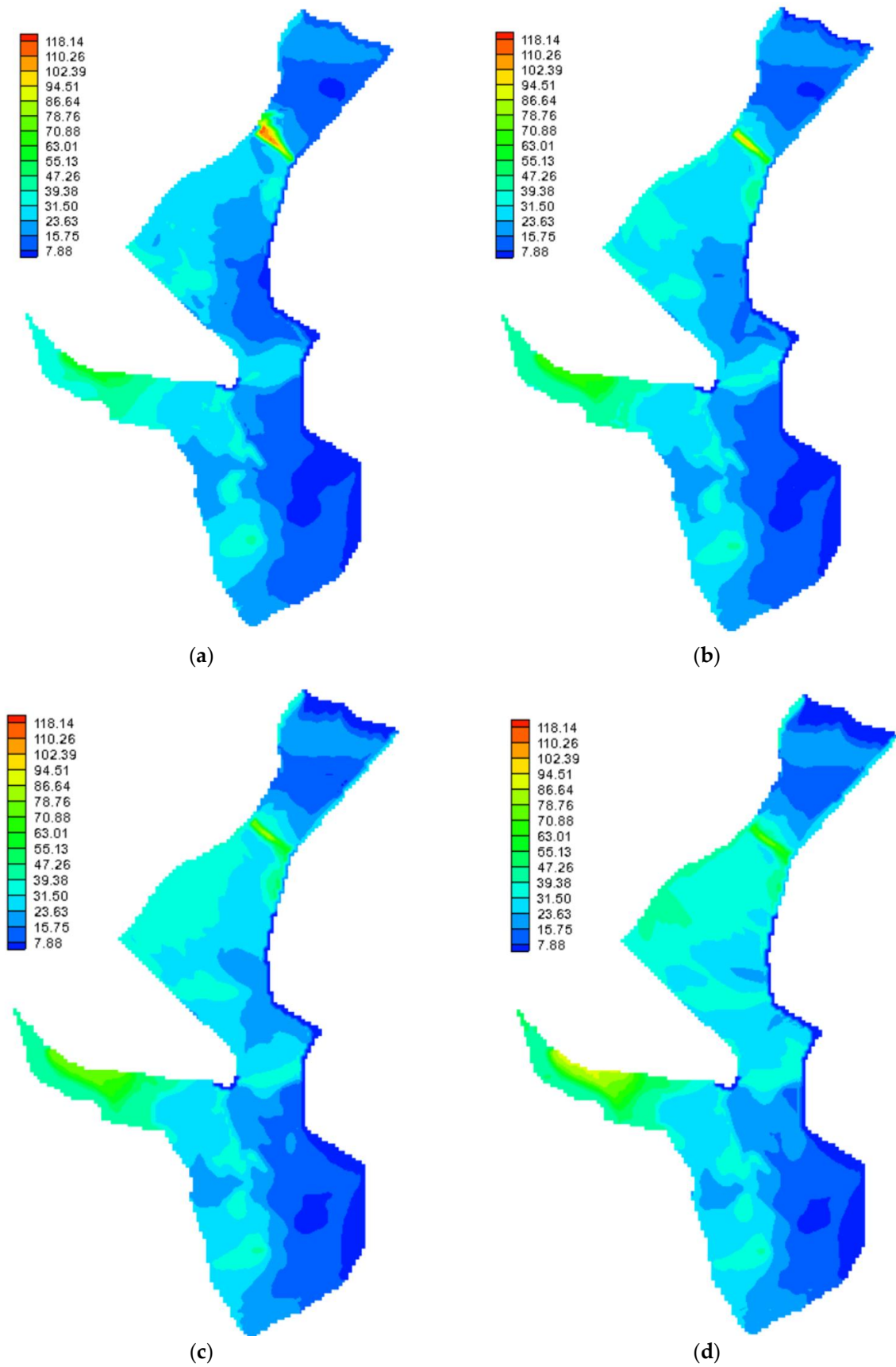


Figure 34. Sodium concentration in the Varamin aquifer: (a) 2025; (b) 2035; (c) 2045; (d) 2055.

3.5.4. Scenario 3: Increase in the Incoming Effluent (TDS) to the Shoor River (50%)

In this scenario, the incoming effluent (TDS) to the Shoor River increased up to 50%. This river is exposed to the industrial activities of the southeastern areas of Tehran Province, since a wastewater treatment plant exists. Therefore, the concentration of TDS added to the Shoor River was investigated. Under this scenario, the TDS concentration will decline by 130.9 milligrams per liter.

Figures 35–38 illustrate a comparison of these different scenarios for the average and maximum changes in the study area.

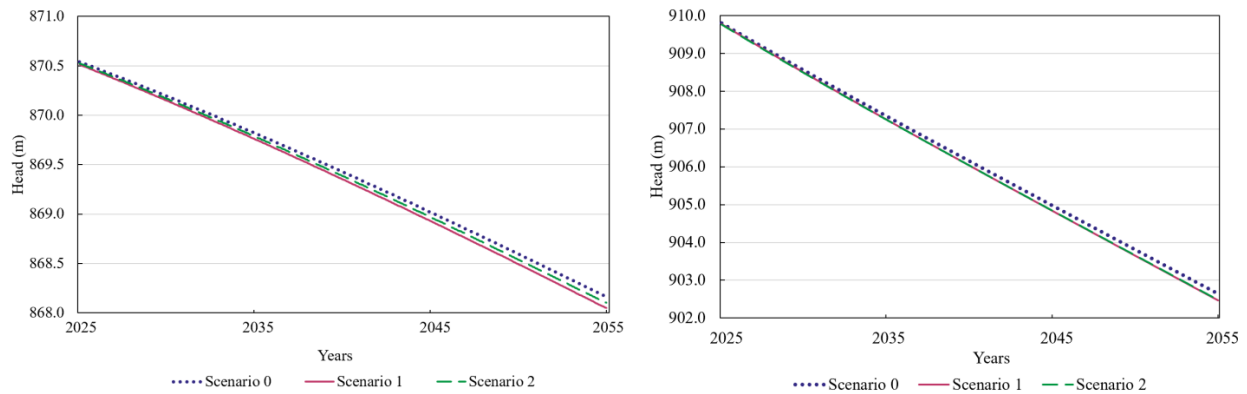


Figure 35. The average (left) and maximum (right) changes in the groundwater level in the aquifer under Scenarios 0, 1, and 2.

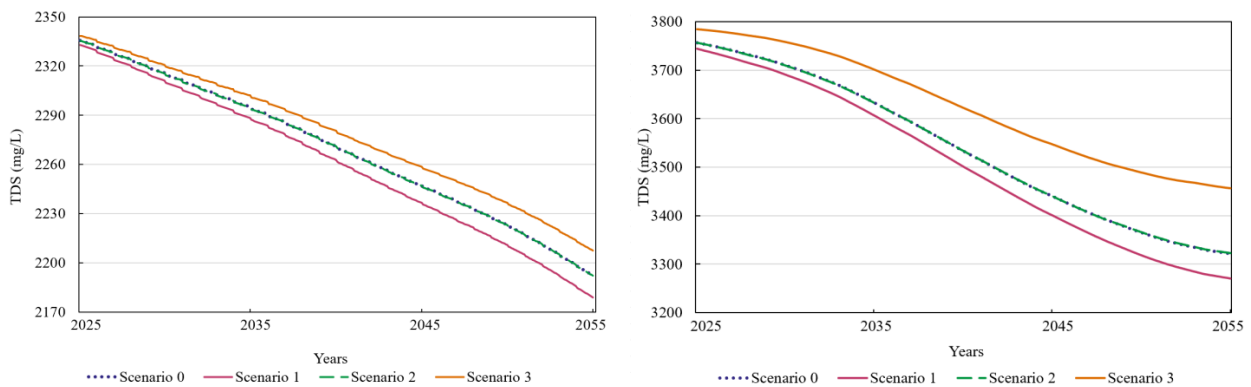


Figure 36. The average (left) and maximum (right) changes in the TDS concentrations in the aquifer under Scenarios 0, 1, 2, and 3.

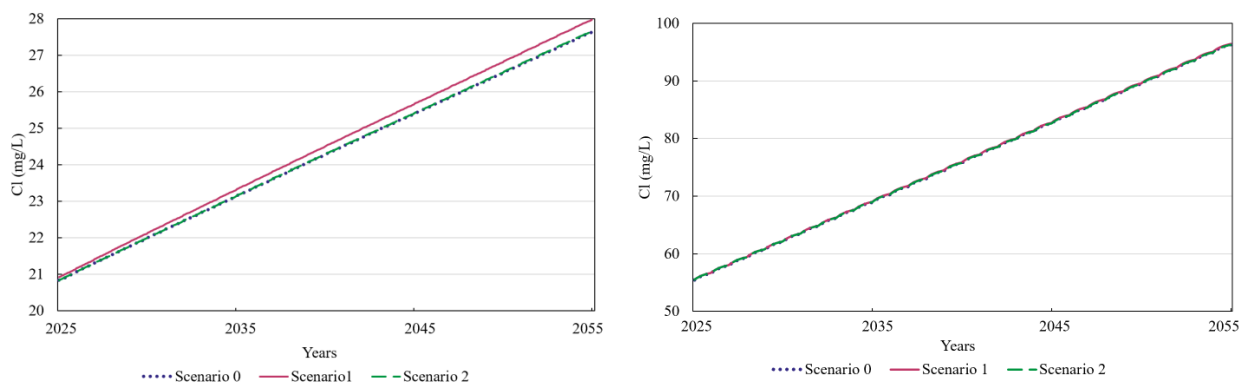


Figure 37. The average (left) and maximum (right) changes in the chloride concentrations in the aquifer under Scenarios 0, 1, and 2.

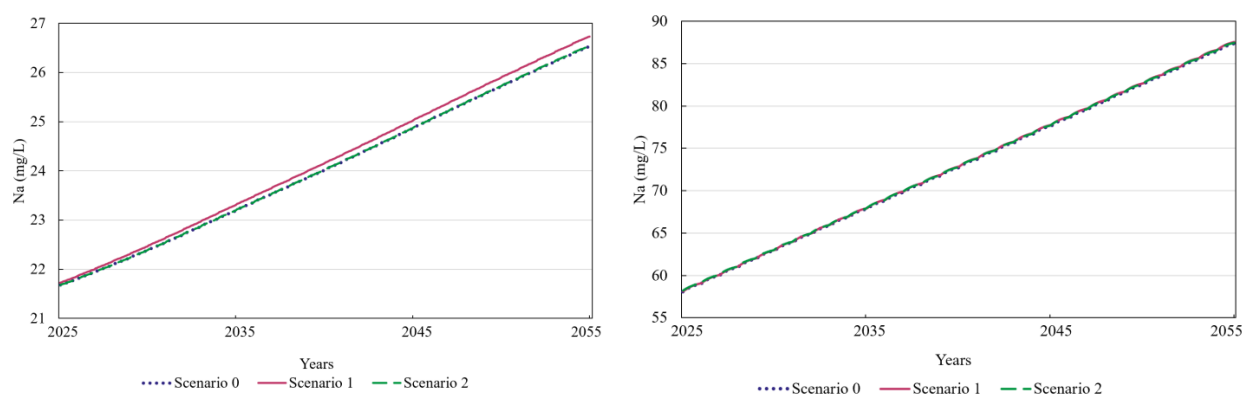


Figure 38. The average (left) and maximum (right) changes in the sodium concentrations in the aquifer under Scenarios 0, 1, and 2.

4. Discussion

The current research aimed to examine the impact of climate change and human effects on alterations in groundwater levels within the western region of the Varamin Plain. Additionally, the study sought to analyze changes in the concentration of certain contaminants, namely, TDS, chloride, and sodium. The rationale behind choosing this particular area was due to the presence of an unapproved elevated level of TDS exceeding 1000 milligrams per liter within this zone.

The modeling was carried out using GMS7.1 software under both steady and unsteady (transient) conditions. The study conducted the steady model analysis for March 2008. At this time, the hydraulic conductivity and surface recharge were subjected to calibration. The calibration outcomes indicate a satisfactory concurrence between the water levels observed and modeled. To clarify, the root mean square error for March 2008 was 1.99 m.

The transient model was also run for eight years, from April 2008 to December 2015, during which the recharge rates and specific yield parameters were calibrated. The findings of the calibration process indicated a very good agreement between the observed and modeled groundwater levels. The Varamin aquifer's groundwater level contour exhibited a decreasing trend from the northern to the southern region, as per the observations made. The validation process for the transient model spanned 24 months from March 2016 to December 2017, during which a satisfactory correspondence was observed between the calculated and observed values.

The subsequent phase of this study involved modeling the contamination transfer in the groundwater of the Varamin Plain. A qualitative model for TDS, chloride, and sodium was implemented on the transient model within the same period. The study involved the calibration of various parameters, including longitudinal and latitudinal dispersion coefficients, porosity, and surface recharge. The findings indicated a satisfactory correlation between the concentrations that were measured and those that were simulated. The concentration of pollutants in the Varamin groundwater aquifer exhibited a declining trend from the western to the eastern regions, as evidenced by the pollutant concentration contours. The model demonstrated an average increase of 2.7 milligrams per liter in chloride concentration, an increase of 2.7 milligrams per liter in sodium concentration, and a decrease of 40.9 milligrams per liter in TDS concentration over an 8-year simulation period. Notably, the qualitative models underwent validation following the transient quantitative model validation period, and the outcomes have demonstrated a reasonable agreement between the modeled and measured values.

The final phase of this investigation entailed an examination of the impacts of climate change and human activities on the Varamin aquifer model during the 30-year interval from 2025 to 2055. In Scenario 0, where the parameters remain constant in the future, the average and maximum groundwater decline at the end of the simulation period will be 2.4 and 7.2 m, respectively. The decrease in the average and maximum TDS concentrations

are equal to 143 and 435 mg/L, respectively. Also, the average concentration of chloride and sodium in this area increases by approximately 7 and 5 mg/L, respectively. For the maximum values, the increase was approximately 41 mg/l for chloride and 29 mg/L for sodium ion.

Under Scenario 1, which involved a 25% increase in pumping, the maximum draw-down reaches 7.3 m. The average and maximum TDS concentration values decrease by 154 and 473 mg/L, while the changes in chloride and sodium concentrations follow the same trend as Scenario 0.

For the climate change scenarios, the maximum groundwater decline was approximately 7.3 m. For the pollutants concentrations, the results were similar to Scenario 0, and the effect of climate change was insignificant on the groundwater quality of this study area.

Finally, Scenario 3, with a 50% increase in incoming effluent (TDS) to the Shoor River, according to industrial activities, was examined. In this scenario, the computed average value of TDS was approximately 2208 mg/L at the end of the simulation period, corresponding to a decrease of 131 mg/L, while the maximum change was about 328 mg/L.

5. Conclusions

In this paper, the effects of climate change and human activities on the groundwater level and the concentration of pollutants, such as total dissolved solids (TDS), chloride, and sodium, were investigated in the western part of the Varamin Plain. For this purpose, four scenarios, including the current condition (Scenario 0), a 25% increase in the extraction from pumping wells (Scenario 1), climate change effects (Scenario 2), and an increase in the incoming effluent (TDS) to the Shoor River because of industrial activities (Scenario 3), were investigated for a future period of 30 years (2025–2055).

The results show that under all scenarios, the concentration of chloride and sodium will increase in the future, but the highest concentration could be observed under Scenario 1 in which the extraction from pumping wells exceeds 25%. Also, the groundwater decline was the most severe under this scenario. The effect of climate change on the concentration of all three pollutants was insignificant.

For the TDS concentration, the decreasing trend observed in the historical period continues in the future for all scenarios. However, under Scenario 3 the lowest decline and under Scenario 1 the highest decline are shown in the simulations.

It should be noted that in this study, there are factors that cause uncertainties which can be categorized into three groups: first, difficulty in predicting the future temperature and precipitation according to the accuracy of the GCM model, the selection of predictors, and the linear relationships between the predictands and the list of predictors; second, the uncertainties exists in the calibration of both the models of MODFLOW and MT3DMS due to the insufficiency of field data in some parts of the plain; and, third, evaluating the response of the aquifer to both the recharge and discharge according to the different components which could alter during the future period (e.g., land use, crop pattern, number of pumping wells, etc.). Because of the uncertainties explained above, the downscaling method should be applied for any other study area, and the set of predictors according to those stations should be selected. However, the results and the set of predictors could be considered as guidelines. It should be stated that the GCM model used in this study should be compared to other models in other areas.

Author Contributions: Conceptualization, R.A., M.Z. and M.E.; methodology, R.A.; software, R.A. and M.Z.; validation, R.A. and M.Z.; formal analysis, R.A. and M.Z.; investigation, R.A. and M.Z.; resources, R.A. and M.Z.; data curation, M.Z.; writing—original draft preparation, R.A. and M.Z.; writing—review and editing, R.A.; visualization, R.A. and M.Z.; supervision, R.A.; project administration, R.A.; funding acquisition, R.A. All authors have read and agreed to the published version of the manuscript.

Funding: This research received no external funding.

Data Availability Statement: The data are not publicly available because of institutional property rights.

Conflicts of Interest: The authors declare no conflict of interest.

References

1. Fetter, C.W. *Applied Hydrogeology*, 4th ed.; PrenticeHall: Englewood Cliffs, NJ, USA, 2001; pp. 1–20.
2. Döll, P.; Hoffmann-Dobrev, H.; Portmann, F.T.; Siebert, S.; Eicker, A.; Rodell, M.; Strassberg, G.; Scanlon, B.R. Impact of water withdrawals from groundwater and surface water on continental water storage variations. *J. Geodyn.* **2012**, *59*, 143–156. [[CrossRef](#)]
3. Hall, N.D.; Stuntz, B.B.; Abrams, R.H. Climate change and freshwater resources. *Nat. Resour. Environ.* **2008**, *22*, 30–35.
4. Li, R.; Merchant, J.W. Modeling vulnerability of groundwater to pollution under future scenarios of climate change and biofuels-related land use change: A case study in North Dakota, USA. *Sci. Total Environ. J.* **2013**, *447*, 32–45. [[CrossRef](#)]
5. Kumar, C.P. Climate change and its impact on groundwater resources. *Int. J. Eng. Sci.* **2012**, *1*, 43–60.
6. Earman, S.; Dettinger, M. Potential impacts of climate change on groundwater resources—A global review. *J. Water Clim. Chang.* **2011**, *2*, 213–229. [[CrossRef](#)]
7. Dragoni, W.; Sukhija, B.S. Climate change and groundwater: A short review. *J. Geol. Soc.* **2008**, *288*, 1–12. [[CrossRef](#)]
8. Taylor, R.G.; Scanlon, B.; Döll, P.; Rodell, M.; Van Beek, R.; Wada, Y.; Longuevergne, L.; Leblanc, M.; Famiglietti, J.S.; Edmunds, M.; et al. Ground water and climate change. *Nat. Clim. Chang.* **2013**, *3*, 322–329. [[CrossRef](#)]
9. Amanambu, A.C.; Obarein, O.A.; Mossa, J.; Li, L.; Ayeni, S.S.; Balogun, O.; Oyebamiji, A.; Ochege, F.U. Groundwater system and climate change: Present status and future considerations. *J. Hydrol.* **2020**, *589*, 125163. [[CrossRef](#)]
10. Pachauri, R.K.; Reisinger, A. *Climate Change 2007: Synthesis Report. Contribution of Working Groups I, II and III to the Fourth Assessment Report of the Intergovernmental Panel on Climate Change*; IPCC: Geneva, Switzerland, 2007; p. 104.
11. Zhou, T.; Wu, P.; Sun, S.; Li, X.; Wang, Y.; Luan, X. Impact of future climate change on regional crop water requirement—A case study of Hetao Irrigation District, China. *Water* **2017**, *9*, 429. [[CrossRef](#)]
12. Goodarzi, M.; Abedi-Koupai, J.; Heidarpour, M. Investigating impacts of climate change on irrigation water demands and its resulting consequences on groundwater using CMIP5 models. *Groundwater* **2019**, *57*, 259–268. [[CrossRef](#)]
13. Elnashar, W.; Elyamany, A. Managing risks of climate change on irrigation water in arid regions. *Water Resour. Manag.* **2023**, *37*, 2429–2446. [[CrossRef](#)]
14. Green, T.R.; Taniguchi, M.; Kooi, H.; Gurdak, J.J.; Allen, D.M.; Hiscock, K.M.; Treidel, H.; Aureli, A. Beneath the surface of global change: Impacts of climate change on groundwater. *J. Hydrol.* **2011**, *405*, 532–560. [[CrossRef](#)]
15. Allen, D.M.; Mackie, D.C.; Wei, M.J.H.J. Groundwater and climate change: A sensitivity analysis for the Grand Forks aquifer, southern British Columbia, Canada. *Hydrogeol. J.* **2004**, *12*, 270–290. [[CrossRef](#)]
16. Allen, D.M.; Cannon, A.J.; Toews, M.W.; Scibek, J. Variability in simulated recharge using different GCMs. *Water Resour. Res.* **2010**, *46*, 1–18. [[CrossRef](#)]
17. Meixner, T.; Manning, A.H.; Stonestrom, D.A.; Allen, D.M.; Ajami, H.; Blasch, K.W.; Brookfield, A.E.; Castro, C.L.; Clark, J.F.; Gochis, D.J.; et al. Implications of projected climate change for groundwater recharge in the western United States. *J. Hydrol.* **2016**, *534*, 124–138. [[CrossRef](#)]
18. Hughes, A.; Mansour, M.; Ward, R.; Kieboom, N.; Allen, S.; Seccombe, D.; Charlton, M.; Prudhomme, C. The impact of climate change on groundwater recharge: National-scale assessment for the British mainland. *J. Hydrol.* **2021**, *598*, 126336. [[CrossRef](#)]
19. Pachauri, R.K.; Allen, M.R.; Barros, V.R.; Broome, J.; Cramer, W.; Christ, R.; Church, J.A.; Clarke, L.; Dahe, Q.; Dasgupta, P.; et al. *Climate Change 2014: Synthesis Report. Contribution of Working Groups I, II and III to the Fifth Assessment Report of the Intergovernmental Panel on Climate Change*; IPCC: Geneva, Switzerland, 2014; p. 151.
20. Swart, N.C.; Cole, J.N.; Kharin, V.V.; Lazare, M.; Scinocca, J.F.; Gillett, N.P.; Anstey, J.; Arora, V.; Christian, J.R.; Hanna, S.; et al. The Canadian earth system model version 5 (CanESM5. 0.3). *Geosci. Model Dev.* **2019**, *12*, 4823–4873. [[CrossRef](#)]
21. Arora, V.K.; Scinocca, J.F.; Boer, G.J.; Christian, J.R.; Denman, K.L.; Flato, G.M.; Kharin, V.V.; Lee, W.G.; Merryfield, W.J. Carbon emission limits required to satisfy future representative concentration pathways of greenhouse gases. *Geophys. Res. Lett.* **2011**, *38*, 1–6. [[CrossRef](#)]
22. Venkataraman, K.; Tummuri, S.; Medina, A.; Perry, J. 21st century drought outlook for major climate divisions of Texas based on CMIP5 multimodel ensemble: Implications for water resource management. *J. Hydrol.* **2016**, *534*, 300–316. [[CrossRef](#)]
23. Chylek, P.; Li, J.; Dubey, M.K.; Wang, M.; Lesins, G.J.A.C. Observed and model simulated 20th century Arctic temperature variability: Canadian earth system model CanESM2. *Atmos. Chem. Phys. Discuss* **2011**, *11*, 22893–22907.
24. Hua, W.; Chen, H.; Sun, S.; Zhou, L. Assessing climatic impacts of future land use and land cover change projected with the CanESM2 model. *Int. J. Climatol.* **2015**, *35*, 3661–3675. [[CrossRef](#)]
25. Hassan, W.H.; Nile, B.K. Climate change and predicting future temperature in Iraq using CanESM2 and HadCM3 modeling. *Model. Earth Syst. Environ.* **2021**, *7*, 737–748. [[CrossRef](#)]
26. Wilby, R.L.; Charles, S.P.; Zorita, E.; Timbal, B.; Whetton, P.; Mearns, L.O. Guidelines for use of climate scenarios developed from statistical downscaling methods. In *Supporting Material of the Intergovernmental Panel on Climate Change, Available from the DDC of IPCC TGCIA*; IPCC: Geneva, Switzerland, 2004.
27. Wilby, R.L.; Dawson, C.W.; Barrow, E.M. SDSM—A decision support tool for the assessment of regional climate change impacts. *Environ. Model. Softw.* **2002**, *17*, 45–157. [[CrossRef](#)]
28. Meenu, R.; Rehana, S.; Mujumdar, P.P. Assessment of hydrologic impacts of climate change in Tunga–Bhadra river basin, India with HEC-HMS and SDSM. *Hydrol. Process.* **2013**, *27*, 1572–1589. [[CrossRef](#)]
29. Wilby, R.L.; Dawson, C.W.; Murphy, C.; Connor, P.O.; Hawkins, E. The statistical downscaling model-decision centric (SDSM-DC): Conceptual basis and applications. *Clim. Res.* **2014**, *61*, 259–276. [[CrossRef](#)]

30. Abbasnia, M.; Toros, H. Future changes in maximum temperature using the statistical downscaling model (SDSM) at selected stations of Iran. *Model. Earth Syst. Environ.* **2016**, *2*, 68. [[CrossRef](#)]
31. Baghanam, A.H.; Eslahi, M.; Sheikhabaei, A.; Seifi, A.J. Assessing the impact of climate change over the northwest of Iran: An overview of statistical downscaling methods. *Theor. Appl. Climatol.* **2020**, *141*, 1135–1150. [[CrossRef](#)]
32. Phuong, D.N.D.; Duong, T.Q.; Liem, N.D.; Tram, V.N.Q.; Cuong, D.K.; Loi, N.K. Projections of future climate change in the Vu Gia Thu Bon River Basin, Vietnam by using statistical downscaling model (SDSM). *Water* **2020**, *12*, 755. [[CrossRef](#)]
33. Eingrüber, N.; Korres, W. Climate change simulation and trend analysis of extreme precipitation and floods in the mesoscale Rur catchment in western Germany until 2099 using Statistical Downscaling Model (SDSM) and the Soil & Water Assessment Tool (SWAT model). *Sci. Total Environ.* **2022**, *838*, 155775.
34. McDonald, M.G.; Harbaugh, A.W. *A Modular Three-Dimensional Finite-Difference Ground-Water Flow Model*; US Geological Survey: Reston, VA, USA, 1988.
35. Harbaugh, A.W.; Banta, E.R.; Hill, M.C.; McDonald, M.G. *Modflow-2000, the U. S. Geological Survey Modular Ground-Water Model-User Guide to Modularization Concepts and the Ground-Water Flow Process*; US Geological Survey: Reston, VA, USA, 2000.
36. Harbaugh, A.W. *MODFLOW-2005, the US Geological Survey Modular Ground-Water Model: The Ground-Water Flow Process*; US Geological Survey: Reston, VA, USA, 2005; Volume 6.
37. Zheng, C.; Wang, P.P. *MT3DMS: A Modular Three-Dimensional Multispecies Transport Model for Simulation of Advection, Dispersion, and Chemical Reactions of Contaminants in Groundwater Systems; Documentation and User's Guide*; U.S. Army Corps of Engineers: Washington, DC, USA, 1999.
38. Owen, S.J.; Jones, N.L.; Holland, J.P. A comprehensive modeling environment for the simulation of groundwater flow and transport. *Eng. Comput.* **1996**, *12*, 235–242. [[CrossRef](#)]
39. Li, R. Assessing groundwater pollution risk in response to climate change and variability. In *Emerging Issues in Groundwater Resources*; Fares, A., Ed.; Springer: Cham, Switzerland, 2016; pp. 31–50.
40. Karami, L.; Alimohammadi, M.; Soleimani, H.; Askari, M. Assessment of water quality changes during climate change using the GIS software in a plain in the southwest of Tehran province, Iran. *Desalination Water Treat.* **2019**, *148*, 119–127. [[CrossRef](#)]
41. Valivand, F.; Katibeh, H. Prediction of nitrate distribution process in the groundwater via 3D modeling. *Environ. Model. Assess.* **2020**, *25*, 187–201. [[CrossRef](#)]
42. Shahvari, N.; Khalilian, S.; Mosavi, S.H.; Mortazavi, S.A. Assessing climate change impacts on water resources and crop yield: A case study of Varamin plain basin, Iran. *Environ. Monit. Assess.* **2019**, *191*, 134. [[CrossRef](#)] [[PubMed](#)]
43. World Health Organization. *Guidelines for Drinking-Water Quality, Health Criteria and Other Supporting Information*, 2nd ed.; World Health Organization: Geneva, Switzerland, 1996; Volume 2.
44. Azizi, H.; Ebrahimi, H.; Mohammad Vali Samani, H.; Khaki, V. Evaluating the effects of climate change on groundwater level in the Varamin plain. *Water Supply* **2021**, *21*, 1372–1384. [[CrossRef](#)]
45. Azizi, H. Development of an integrated multi-objective approach to formulate optimal harvesting policies with the aim of sustainable management of groundwater resources: Study area: Varamin Plain. *J. Hydroinf.* **2023**, *25*, 469–490. [[CrossRef](#)]
46. Karami, S.; Madani, H.; Katibeh, H.; Marj, A.F. Assessment and modeling of the groundwater hydrogeochemical quality parameters via geostatistical approaches. *Appl. Water Sci.* **2018**, *8*, 23. [[CrossRef](#)]
47. TRWA. *Report of Groundwater Resources Studies in Varamin Area (in Persian)*; Tehran Regional Water Authority: Tehran, Iran, 2014.
48. Bedient, P.B.; Rifai, H.S.; Newell, C.J. *Ground Water Contamination: Transport and Remediation*, 1st ed.; Prentice-Hall International Inc.: Englewood Cliffs, NJ, USA, 1994; pp. 119–144.
49. Hargreaves, G.H. Defining and using reference evapotranspiration. *J. Irrig. Drain. Eng.* **1994**, *120*, 1132–1139. [[CrossRef](#)]
50. Brouwer, C.; Heibloem, M. *Irrigation Water Management Training Manual No.3: Irrigation Water Needs*; Food and Agriculture Organization of the United Nations (FAO): Rome, Italy, 1986.
51. Almasri, M.N.; Kaluarachchi, J.J. Modeling nitrate contamination of groundwater in agricultural watersheds. *J. Hydrol.* **2007**, *343*, 211–229. [[CrossRef](#)]

Disclaimer/Publisher's Note: The statements, opinions and data contained in all publications are solely those of the individual author(s) and contributor(s) and not of MDPI and/or the editor(s). MDPI and/or the editor(s) disclaim responsibility for any injury to people or property resulting from any ideas, methods, instructions or products referred to in the content.